

PARAMETRIC STUDY OF GAS TURBINE FILM-COOLING

A Dissertation

by

KEVIN LIU

Submitted to the Office of Graduate Studies of
Texas A&M University
in partial fulfillment of the requirements for the degree of

DOCTOR OF PHILOSOPHY

August 2012

Major Subject: Mechanical Engineering

Parametric Study of Gas Turbine Blade Film-Cooling

Copyright 2012 Kevin Liu

PARAMETRIC STUDY OF GAS TURBINE FILM-COOLING

A Dissertation

by

KEVIN LIU

Submitted to the Office of Graduate Studies of
Texas A&M University
in partial fulfillment of the requirements for the degree of

DOCTOR OF PHILOSOPHY

Approved by:

Chair of Committee,	Je-Chin Han
Committee Members,	Gerald L. Morrison
	Eric L. Petersen
	Hamn-Ching Chen
Head of Department,	Jerald A. Caton

August 2012

Major Subject: Mechanical Engineering

ABSTRACT

Parametric Study of Gas Turbine Film-Cooling. (August 2012)

Kevin Liu, B.S., Kansas State University;

M.S., Texas A&M University

Chair of Advisory Committee: Dr. Je-Chin Han

In this study, the film-cooling effectiveness in different regions of gas turbine blades was investigated with various film hole/slot configurations and mainstream flow conditions. The study consisted of three parts: 1) turbine blade span film-cooling, 2) turbine platform film-cooling, and 3) blade tip film-cooling. Pressure sensitive paint (PSP) technique was used to get the conduction-free film-cooling effectiveness distribution. Film-cooling effectiveness is assessed in terms of cooling hole geometry, blowing ratio, freestream turbulence, and coolant-to-mainstream density ratio.

Blade span film-cooling test shows that the compound angle shaped holes offer better film effectiveness than the axial shaped holes. Greater coolant-to-mainstream density ratio prevents coolant to lift-off. Higher freestream turbulence causes effectiveness to drop everywhere except in the region downstream of suction side. Results are also correlated with momentum flux, compound shaped hole has the greatest optimum momentum flux ratio, and then followed by axial shaped hole, compound cylindrical hole, and axial cylindrical hole.

For platform purge flow cooling, the stator-rotor gap was simulated by a typical labyrinth-like seal. Two different film-cooling hole geometries, three blowing ratios and

density ratios, and two freestream turbulence are examined. Results showed that the shaped holes present higher film-cooling effectiveness and wider film coverage than the cylindrical holes, particularly at higher blowing ratios. Moreover, the platform film-cooling effectiveness increases with density ratio but decreases with turbulence intensity.

The blade tip study was performed in a blow-down flow loop. Results show that a blowing ratio of 2.0 is found to give best results on the tip floor. Lift-off of the coolant jet can be observed for the holes closer to the leading edge as blowing ratio increases from 1.5 to 2.0.

A stator vane suction side heat transfer study was conducted in a partial annular cascade. The heat transfer coefficients were measured by using the transient liquid crystal technique. At $X/L=0.15$, a low heat transfer region where transition occurs. The heat transfer coefficients increase toward the trailing edge as flow accelerates; a spanwise variation can be found at neat tip and hub portions due to passage and horseshoe vortices.

DEDICATION

To my parents and sister for their endless love, support, and encouragement.

ACKNOWLEDGEMENTS

I would like to express my deepest appreciation to Dr. Je-Chin Han, the chair of my doctoral committee, for his support and guidance to complete this research successfully. I am appreciative that Dr. Gerald Morrison, Dr. Eric Petersen, and Dr. Hamn-Ching Chen have served on my committee and gave me suggestions on my research and dissertation. I also thank all the experienced partners in the lab who always gave me helpful advice and solutions.

NOMENCLATURE

A	Area (m^2)
B	Turbulence grid bar width (cm)
C	Oxygen concentration
C_x	Axial chord length of the blade
d	Diameter of film-cooling holes (mm)
DR	Coolant-to-mainstream density ratio
h	Blade span (cm) or heat transfer coefficient ($\text{W}/\text{m}^2 \text{K}$)
H	Cascade height (cm)
I	Pixel intensity for an image or Momentum ratio of coolant ($= M^2/\text{DR}$)
K	Thermal conductivity ($\text{W}/\text{m K}$)
l	length of the film-cooling hole (cm)
\dot{m}	Mass flow rate (kg/s)
M	Average blowing ratio ($= \rho_c V_c / \rho_m V_m$)
Ma	Mach number
MFR	Mass flow ratio of slot purge flow ($= \dot{m}_{\text{purge}} / \dot{m}_m$)
P	Local static pressure (Pa)
P_t	Total pressure (Pa)
P_{O_2}	Partial pressure of oxygen (Pa)

Re	Reynolds number
s	Distance between adjacent holes in a hole row
S	Blade pitch (cm)
t	Transient time for liquid crystal color change
T	Temperature (K)
Tu	Turbulence intensity level at the cascade inlet
V	Velocity (m/s)
W	Molecular weight (kg/kmol)
x	Axial distance measured from blade leading edge (cm)
y	Pitchwise distance along blade span measured from hub (cm)
z	Spanwise distance measured from platform (cm)
α	Thermal diffusivity (m^2/s)
η	Film-cooling effectiveness
ρ	Density of fluid (kg/m^3)

Subscript

air	Mainstream air with air as coolant
aw	Adiabatic wall
blk	Image without illumination (black)
c	Coolant
ex	Exit of cascade
f	Local film

i	Initial
in	Inlet of cascade
m	Mainstream
mix	Mainstream air with foreign gas coolant
r	Coolant hole row
ref	Reference image with no mainstream and coolant flow
w	Wall

Acronyms

LE	Leading edge of the blade
PS	Pressure side
SS	Suction side
ST	Stagnation

TABLE OF CONTENTS

	Page
ABSTRACT	iii
DEDICATION.....	v
ACKNOWLEDGEMENTS	vi
NOMENCLATURE	vii
TABLE OF CONTENTS	x
LIST OF FIGURES.....	xii
LIST OF TABLES.....	xv
1. INTRODUCTION.....	1
2. MEASUREMENT THEORY AND DATA ANALYSIS	4
2.1. Pressure Sensitive Paint	4
2.2. Transient Liquid Crystal Technique	9
3. TURBINE BLADE SPAN FILM-COOLING	11
3.1. Introduction	11
3.2. Experimental Setup	13
3.3. Results and Discussion.....	21
3.3.1. Effect of Blowing Ratio	21
3.3.2. Effect of Density Ratio.....	27
3.3.3. Effect of Freestream Turbulence Intensity	32
3.3.4. Effect of Momentum Flux Ratio	37
3.4. Conclusions	39
4. TURBINE BLADE PLATFORM FILM-COOLING	41
4.1. Introduction	41
4.2. Experimental Setup	44
4.3. Results and Discussion.....	51
4.3.1. Pressure Measurement on Platform.....	51

	Page
4.3.2. Adiabatic Film-Cooling Effectiveness	51
4.3.3. Effect of Density Ratio.....	53
4.3.4. Effect of Blowing Ratio	56
4.3.5. Effect of Freestream Turbulence Intensity	56
4.3.6. Laterally Average Film-Cooling Effectiveness	61
4.4. Conclusions	65
5. TURBINE BLADE TIP FILM-COOLING.....	66
5.1. Introduction	66
5.2. Experimental Setup	67
5.3. Results and Discussion.....	72
5.3.1. Film-Cooling Effectiveness Results.....	72
5.3.2. Average Film-Cooling Effectiveness Results.....	72
5.4. Conclusions	73
6. VANE SUCTION SIDE HEAT TRANSFER STUDY	77
6.1. Objectives of Vane Suction Side Heat Transfer	77
6.2. Test Facilities for Heat Transfer Study.....	77
6.3. Results and Discussion.....	80
6.3.1. Surface Initial Temperature	80
6.3.2. Heat Transfer Coefficient Results	80
6.4. Conclusions	82
7. SUMMARY	83
REFERENCES.....	85
VITA.....	93

LIST OF FIGURES

		Page
Figure 1.1	Typical gas turbine blade cooling scheme (a) internal cooling; (b) external cooling	3
Figure 2.1	PSP working principle.....	5
Figure 2.2	PSP calibration setup and calibration curves.....	5
Figure 2.3	Transient liquid crystal working principle	8
Figure 2.4	Heat transfer coefficient measurement theory: 1D semi-infinite solid model	8
Figure 3.1	Schematic of experimental facility.....	14
Figure 3.2	Optical setup.....	15
Figure 3.3	Details of the test blade (Axial shaped hole).....	16
Figure 3.4	Details of the test blade (Compound shaped hole).....	17
Figure 3.5	Adiabatic effectiveness distribution at three different blowing ratios (Axial shaped hole)	23
Figure 3.6	Spanwise average adiabatic effectiveness as a function of blowing ratio (Axial shaped hole).....	24
Figure 3.7	Adiabatic effectiveness distribution at three different blowing ratios (Compound shaped hole).....	25
Figure 3.8	Spanwise average adiabatic effectiveness as a function of blowing ratio (Compound shaped hole).....	26
Figure 3.9	Adiabatic effectiveness distribution at three different density ratios (Axial shaped hole)	28
Figure 3.10	Spanwise average adiabatic effectiveness as a function of density ratio (Axial shaped hole).....	29

	Page
Figure 3.11 Adiabatic effectiveness distribution at three different density ratios (Compound shaped hole).....	30
Figure 3.12 Spanwise average adiabatic effectiveness as a function of density ratio (Compound shaped hole)	31
Figure 3.13 Adiabatic effectiveness distribution at two different freestream turbulence intensities (Axial shaped hole)	33
Figure 3.14 Spanwise average adiabatic effectiveness as a function of freestream turbulence intensity (Axial shaped hole).....	34
Figure 3.15 Adiabatic effectiveness distribution at two different freestream turbulence intensities (Compound shaped hole)	35
Figure 3.16 Spanwise average adiabatic effectiveness as a function of freestream turbulence intensity (Compound shaped hole).....	36
Figure 3.17 Comparison of laterally-average effectiveness	38
Figure 4.1 Schematic of test section facility.....	45
Figure 4.2 Schematic of cascade blade platform	47
Figure 4.3 Blade platform film-cooling slot and discrete hole.....	47
Figure 4.4 Pressure and Mach number distribution without coolant injection.....	52
Figure 4.5 Density ratio effect on adiabatic film-cooling effectiveness for Config. A (a) DR=1.0, (b) DR=1.5, (c) DR=2.0.....	54
Figure 4.6 Density ratio effect on adiabatic film-cooling effectiveness for Config. B (a) DR=1.0, (b) DR=1.5, (c) DR=2.0	55
Figure 4.7 Blowing ratio effect on adiabatic film-cooling effectiveness for Config. A (a) M=1.0, (b) M=1.5, (c) M=2.0	57
Figure 4.8 Blowing ratio effect on adiabatic film-cooling effectiveness for Config. B (a) M=1.0, (b) M=1.5, (c) M=2.0	58

	Page
Figure 4.9 Turbulence intensity effect on adiabatic film-cooling effectiveness for Config. A (a) $Tu=4.2\%$, (b) $M=10.5\%$	59
Figure 4.10 Turbulence intensity effect on adiabatic film-cooling effectiveness for Config. B (a) $Tu=4.2\%$, (b) $M=10.5\%$	60
Figure 4.11 Laterally averaged effectiveness for Config. A (a) density ratio effect, (b) blowing ratio effect, (c) turbulence effect	63
Figure 4.12 Laterally averaged effectiveness for Config. B (a) density ratio effect, (b) blowing ratio effect, (c) turbulence effect	64
Figure 5.1 Schematic of test section and blow down facility	69
Figure 5.2 Definition of blade tip and shroud.....	69
Figure 5.3 Internal passage geometry of test blade	70
Figure 5.4 Orientation of tip and PS holes	71
Figure 5.5 Film-cooling effectiveness distribution on blade tip.....	74
Figure 5.6 Averaged film-cooling effectiveness from experimental results.....	75
Figure 5.7 Area-averaged film-cooling effectiveness from experimental results	76
Figure 6.1 Test vane (a) hole locations (b) coolant passage	79
Figure 6.2 Schematic of setup for vane suction side film-cooling and heat transfer study	79
Figure 6.3 Initial temperature on stator vane suction side.....	81
Figure 6.4 Heat transfer coefficient on the vane suction side	81

LIST OF TABLES

	Page
Table 3.1 Cascade geometry and mainstream flow conditions for blade span film-cooling.....	19
Table 3.2 Summary of experimental conditions for blade span film-cooling.....	20
Table 4.1 Cascade geometry and mainstream flow conditions for blade platform film-cooling.....	49
Table 4.2 Summary of experimental conditions for blade platform film-cooling.....	50

1. INTRODUCTION

To improve thermal efficiency, advanced gas turbines operate at high rotor inlet temperatures; the high inlet temperature creates thermal stresses on the blades which can be detrimental to the operation of the engine. In order to achieve reasonable durability goals, improved cooling techniques are applied to turbine blades. A comprehensive review of turbine blade heat transfer and cooling techniques can be found in the book by Han et al. [1]. Gas turbine cooling techniques have been studied for many years. However, as the engines become more advanced, designers require more information to develop efficient cooling schemes. One of commonly used cooling techniques in modern high temperature gas turbine engines is film-cooling to reduce the heat flux into the blade from the hot mainstream. Figure 1 shows a typical film-cooled blade. In general, the discrete film cooling holes are employed on the blade leading edge, blade tip, pressure and suction surface to meet both the cooling and structural requirement. The slot film cooling is usually applied to the blade trailing edge and platform. Sometimes, the discrete-holes film-cooling is also applied to the downstream of turbine platform to provide additional film protection for the platform.

The film-cooling techniques have been studied for many years. However, film-cooling performance in gas turbine engines is influenced by the film-cooling hole configuration as well as the freestream flow condition. In term of film-cooling hole configurations, these effects include the film-cooling hole geometries (continuous slot or

This dissertation follows the style of ASME Journal of Turbomachinery.

discrete holes, straight hole or expanded hole), hole orientations (simple angle or compound angle), the internal cooling supply (passage or plenum) and so on. As the film-cooling is a result of interaction of mainstream flow cooling performance. The freestream effects include the freestream turbulence, unsteady wake, passage vortices, the blowing ratio, density ratio. In addition the film performance also depends on the surface curvature, surface roughness, etc. Depending on the regions in the turbine blade and the local mainstream flow characteristic, the film-cooling design varies. In this study, the film-cooling effectiveness will be investigated for different portions of the turbines blades and vane with different emphasis as listed below.

1. Film-cooling effectiveness on a fully film-cooled high pressure turbine blade surface.
2. The platform cooling by purge flow from a simulated stator-rotor seal combined with discrete-hole film-cooling within the blade passage.
3. Film-cooling effectiveness of a high pressure gas turbine blade tip in transonic flow conditions.
4. Heat transfer on a vane suction side surface with transonic flow condition.

Various mainstream turbulence intensities, discrete film-cooling blowing ratios, slot-cooling mass flow ratio, and coolant-to-mainstream density ratios are investigated. Detailed film-cooling effectiveness measurements will be measured using pressure sensitive paint (PSP) techniques. Surface heat transfer measurement will be investigated using transient liquid crystal (TLC) method.

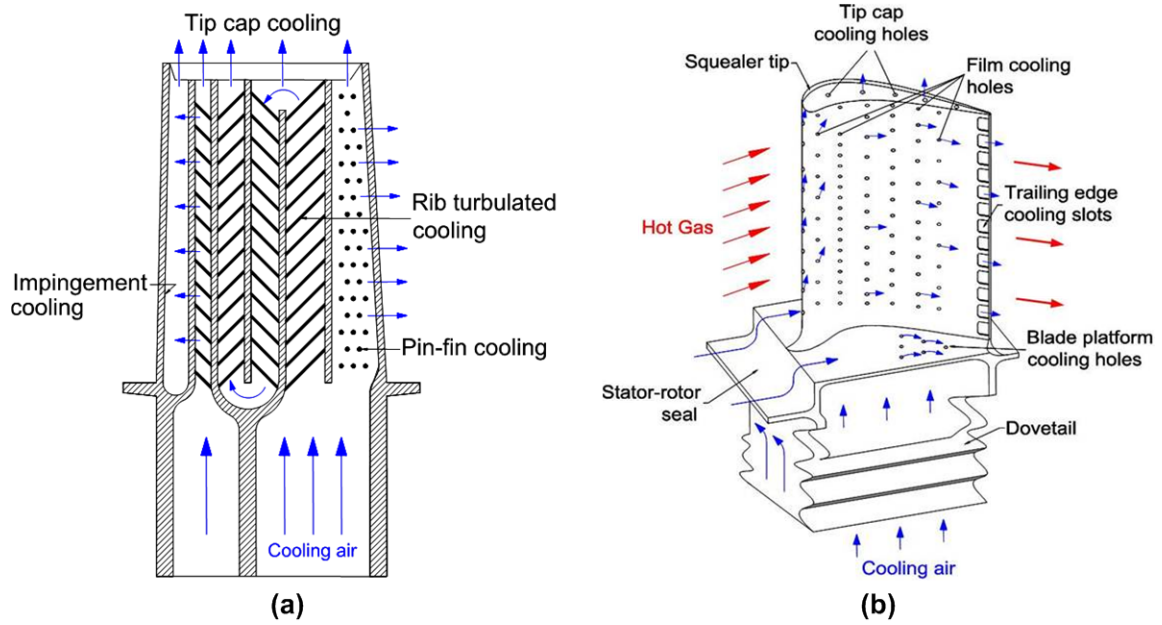


Figure 1.1 Typical gas turbine blade cooling scheme (a) internal cooling; (b) external cooling

2. MEASUREMENT THEORY AND DATA ANALYSIS

2.1. Pressure Sensitive Paint

Data for film-cooling effectiveness were obtained by using the PSP technique. PSP is a photo-luminescent material that emits light when excited, with the emitted light intensity inversely proportional to the partial pressure of oxygen (i.e., oxygen quenching). Figure 2.1 shows the PSP working principle. This emitted light intensity was recorded using a CCD camera. Details of using PSP for pressure measurements are given in McLachlan and Bell [2]. The image intensity (I) recorded in the presence of mainstream air and coolant (wind-on condition) was normalized with a reference image intensity (I_{ref}) taken under no-flow condition (wind-off condition). Background noise in the camera was removed by subtracting both these image intensities with the image intensity (I_{blk}) obtained under no-flow condition and without light excitation. The resulting intensity ratio was converted to pressure ratio using a pre-determined calibration curve and expressed as:

$$\frac{I_{ref} - I_{blk}}{I - I_{blk}} = f \left(\frac{(P_{O_2})_{air}}{(P_{O_2})_{ref}} \right) = f(P_{ratio}) \quad (1)$$

where I denotes the intensity obtained for each pixel and $f(P_{ratio})$ is the relationship between intensity ratio and pressure ratio obtained after calibration.

Calibration of PSP system was performed using a vacuum chamber at several known pressures varying from 0 to 1.8atm. The calibration curve and a schematic of the optical component setup are shown in Figure 2.2. The same optical setup that was used

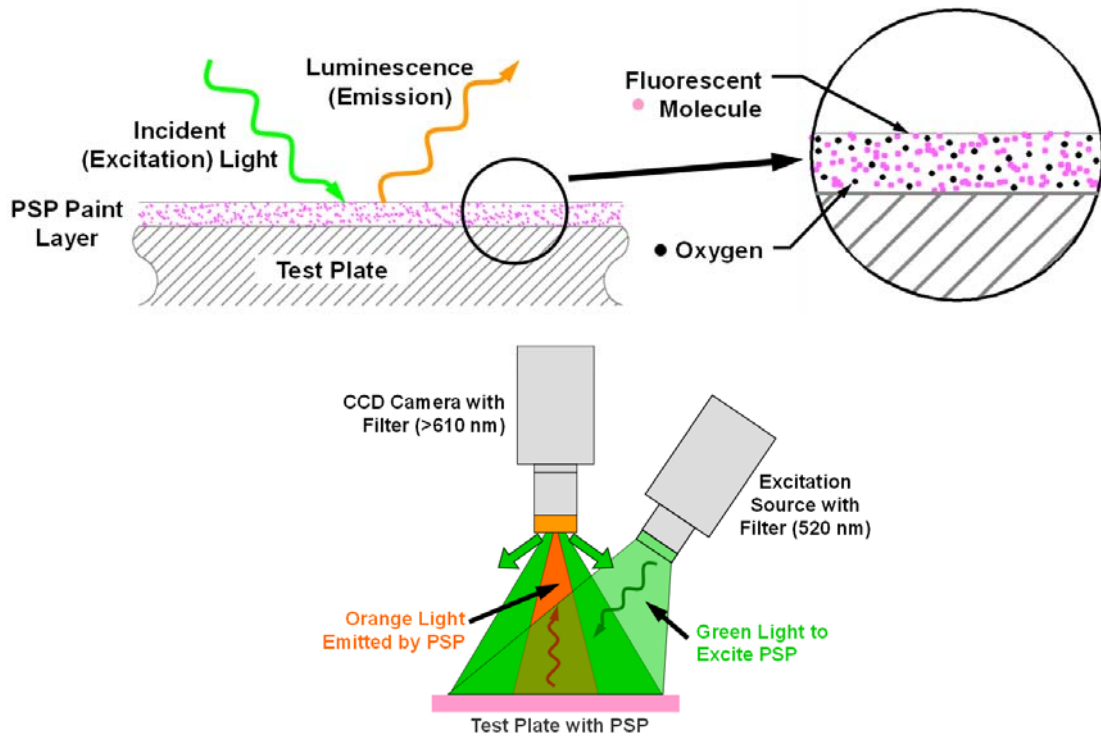


Figure 2.1 PSP working principle

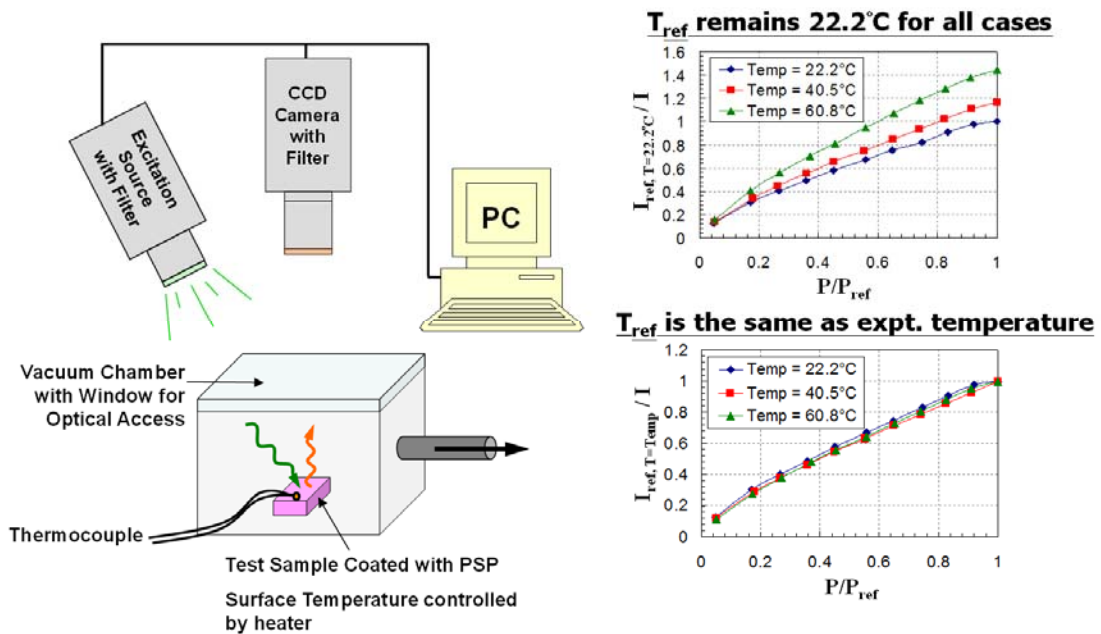


Figure 2.2 PSP calibration setup and calibration curves

during experiments was chosen for calibration. PSP is sensitive to temperature as well with higher temperatures resulting in lower light emission. It was however observed that if the emitted light intensity (I) recorded at a certain temperature was normalized with the reference image intensity (I_{ref}) taken at the same temperature (Equation2), the temperature sensitivity could be minimized to a great extent. Hence, during experiments, the reference (I_{ref}) and black (I_{blk}) images were acquired immediately after stopping the mainstream flow when the temperature of the blade surface did not change appreciably from the wind-on case.

To obtain film cooling effectiveness, air and foreign gas were used alternately as coolant. Foreign gas displaces the oxygen molecules on the surface causing a change in the emitted light intensity from PSP. By noting the difference in partial pressure between the air and nitrogen injection cases, the film cooling effectiveness was determined using the following equation.

$$\eta = \frac{T_{mix} - T_m}{T_c - T_m} = \frac{C_{mix} - C_{air}}{C_{N_2} - C_{air}} = 1 - \frac{1}{\left[\frac{(P_{O_2})_{,air}}{(P_{O_2})_{,mix}} - 1 \right] \frac{W_{fg}}{W_{air}} + 1} \quad (2)$$

where C_{air} , C_{mix} and C_{N_2} are the oxygen concentrations of mainstream air, air/foreign gas mixture and nitrogen on the test surface, respectively.

The accuracy of the PSP technique for measuring film-cooling effectiveness has been compared by Wright et al. [3] on a flat plate with compound angle ejection holes using steady-state Infra-Red (IR) technique and steady-state Temperature Sensitive Paint (TSP) technique. Results were obtained for a range of blowing ratios and showed an

agreement within 15% of each other. Larger uncertainties for heat transfer techniques such as IR and TSP methods were due to lateral heat conduction in the flat plate as corrections for heat conduction were not included in the presented results.

The test blade under investigation was coated with PSP using an air brush. It was then excited using a strobe light fitted with a narrow band-pass interference filter (optical wavelength is 520nm). A flexible dual fiber optic guide was used to get a uniform incident light distribution on the test surface. Upon excitation, the PSP coated surface emitted light with a wavelength higher than 600nm. A 12-bit scientific grade CCD camera (Cooke Sensicam QE with CCD temperature maintained at -15°C using 2-stage peltier cooler) was used to record images and was fitted with a 35mm lens and a 600nm long-pass filter. The filter mounted on the camera was chosen such that any stray light would not pass through. The camera and the strobe light were triggered simultaneously using a TTL signal from a function generator. A total of 200 TIF images were captured and ensemble-averaged to get the emission intensities. The spatial resolution of each image was 0.6mm/pixel. A computer program was used to convert the pixel intensities into pressure (using the calibration curve) and finally into film-cooling effectiveness.

Uncertainty calculations have been performed based on the uncertainty analysis method of Kline and McClintock [4] and Colemand and Steele [5]. The uncertainty in adiabatic effectiveness amounts to $\pm 1\%$ for $\eta=0.3$ and $\pm 8\%$ for $\eta=0.05$.

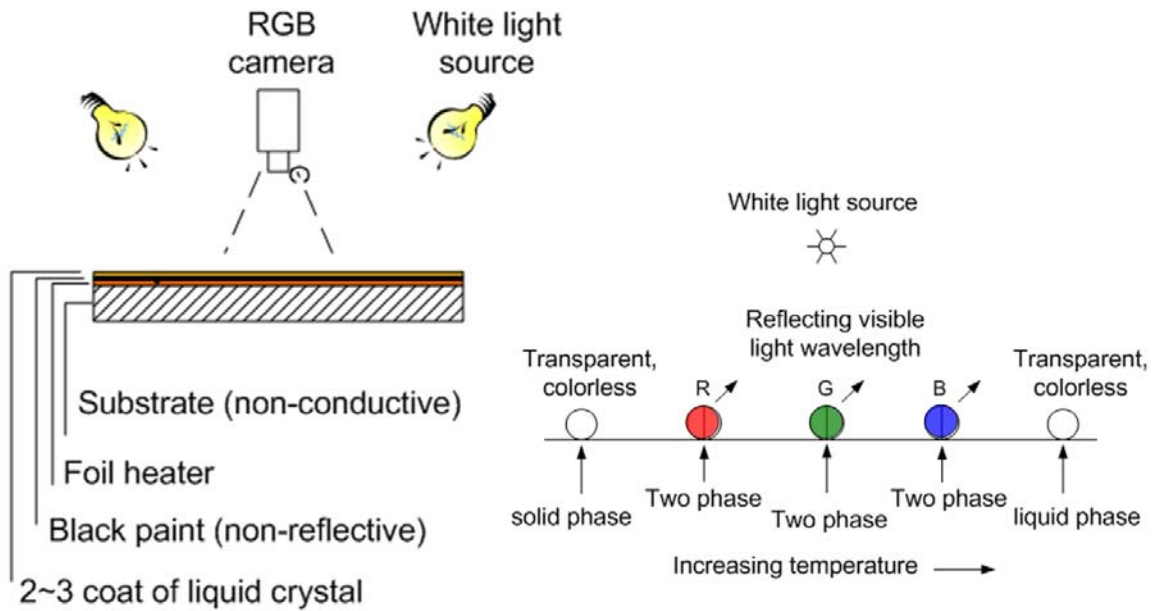


Figure 2.3. Transient liquid crystal working principle

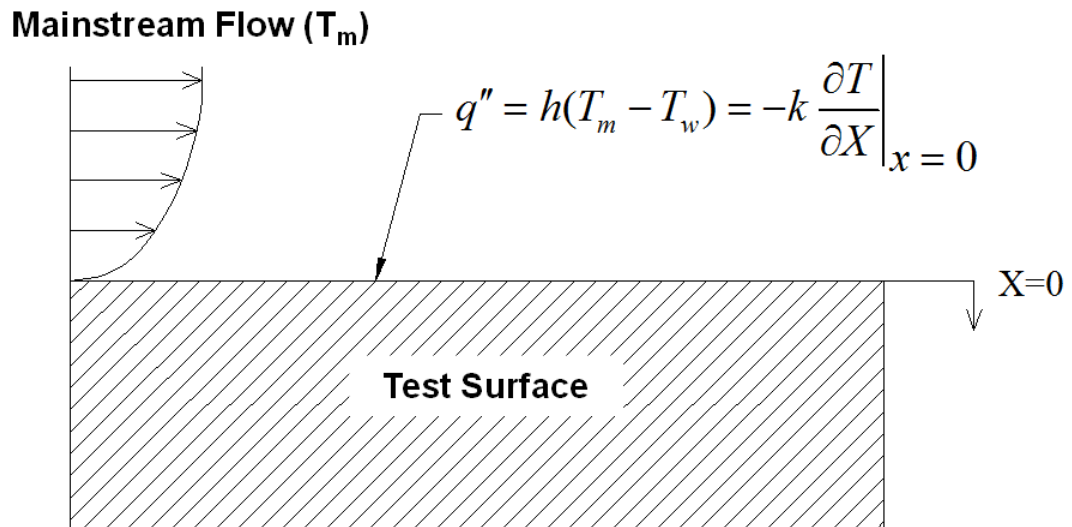


Figure 2.4. Heat transfer coefficient measurement theory: 1D semi-infinite solid model

2.2. Transient Liquid Crystal Technique

A hue detection based transient liquid crystals technique, shown in Figure 2.3, was used to measure heat transfer and film-cooling effectiveness on the surface. The local heat transfer coefficient over a liquid crystals coated surface without film injection can be obtained using a 1- dimensional semi-infinite solid assumption for the test surface, shown in Figure 2.4. Note that the blade material (SLA) has a low thermal conductivity of 0.47W/m K. The test duration is smaller (10-30 sec) than the time required for the temperature to penetrate the full thickness of the blade tip material. Thus a 1-D transient, semi-infinite solid assumption is valid throughout the surface, except near the tip edges. The local heat transfer coefficient over a TLC coated surface can be obtained using a 1-dimensional semi-infinite solid assumption with convective boundary condition at the test surface.

$$k \frac{\partial^2 T}{\partial x^2} = \rho C_p \frac{\partial T}{\partial t}$$

$$at t = 0, T = T_i$$

$$at x = 0, -k \frac{\partial T}{\partial x} = h(T_w - T_m)$$

$$at x \rightarrow \infty, T = T_i$$
(3)

The solution for the above 1-D transient conduction equation at the surface (x=0) is:

$$\frac{T_w - T_i}{T_m - T_i} = 1 - \exp\left(\frac{h^2 \alpha t}{k^2}\right) \operatorname{erfc}\left(\frac{h\sqrt{\alpha t}}{k}\right)$$
(4)

By knowing the initial temperature (T_i) of the test surface, the mainstream (recovery) temperature (T_m) at the cascade inlet and the color change temperature (T_w) at time t , the local heat transfer coefficient (h) can be calculated from Equation (4). For the film-cooling test, the mainstream temperature (T_m) in Equation (5) is replaced by the local film temperature (T_f), which is a mixture of the coolant (T_c) and mainstream temperature (T_m). The film temperature is defined in terms of the film-cooling effectiveness η .

$$\eta = \frac{T_w - T_i}{T_m - T_i} \quad \text{or} \quad T_f = \eta T_c + (1 - \eta) T_m \quad (5)$$

Then, Equations (5) and (6) can be combined as follows:

$$\frac{T_w - T_i}{T_f - T_i} = \frac{T_w - T_i}{\eta T_c + (1 - \eta) T_m - T_i} = 1 - \exp\left(\frac{h^2 \alpha t}{k^2}\right) \operatorname{erfc}\left(\frac{h \sqrt{\alpha t}}{k}\right) \quad (6)$$

The experimental uncertainty was calculated by the methods of Kline and McClintock [4]. The uncertainty for the local heat transfer coefficient and film-cooling effectiveness was estimated to be 8% and 10%, respectively.

3. TURBINE BLADE SPAN FILM-COOLING

3.1. Introduction

In an attempt to understand benefits of film-cooling with different film-cooling hole configurations, many studies were performed on a flat plate. Goldstein et al. [6] showed the benefits of film-cooling with shaped holes. The findings [7, 8] also showed that for film-cooling hole with expended exit, a reduction of mean velocity of the coolant causing the jet to stay closer to the surface. As a result, a significant increase in film-cooling effectiveness was evidenced. Dittmar et al. [9], conducted measurements on a model of a suction side of an actual turbine guide vane. According to their study, fan-shaped holes provided good effectiveness values at moderate and high blowing ratios unlike the cylindrical holes which suffered from jet separation. The effect of surface curvature was investigated by Ito et al. [10], they reported higher effectiveness on a convex surface than on a flat plate; whereas the opposite trend is discovered on the concave wall. Chen et al. [11] also investigated film-cooling effectiveness on both axial and compound shaped holes. Bunker [12] spent the effort on examining the origins of shaped film-cooling and summarizes the extant literature knowledge concerning the performance of such film holes. Ekkad et al. [13] used two coolant densities to demonstrate that turbulence decreases the film-cooling effectiveness. The high density coolant produced higher effectiveness and attained peak effectiveness at higher blowing ratio. Similar conclusion was made by Wayne et al. [14] testing on the suction side of the stator vane. Recently, several studies [15, 16] conducted with film-cooling holes

embedded in a trench have shown improvement of effectiveness. This configuration is characterized by inclined film-cooling holes which inject the coolant into a trench for better lateral spreading on the airfoil surface. Colban et al. [17] determined the physical relationship between film-cooling effectiveness and several parameters, such as blowing ratio, hole coverage ratio, area ratio, and hole spacing. They made a correlation for predicting adiabatic film-cooling effectiveness downstream of a single row of shaped holes on a flat-plate surface. More recently, Mhetras et al. [18] observed the excellent coolant coverage offered by compound shaped holes near the tip region of the pressure side. Their study showed that the shaped holes on the pressure side of the blade could be utilized in cooling the cut-back region of the tip cavity floor. Effect of a rotating, unsteady wake on film cooling effectiveness and coolant jet temperature profiles on the suction side of a turbine blade were investigated by Ou et al. [19] over a linear turbine blade cascade with film-cooling. A spoked-wheel mechanism was used to generate the upstream wakes. They tested no-wake case and wake Strouhal numbers of 0.1 and 0.3. Air and CO₂ were used to study effect of density ratio. It was found that increasing wake passing frequency increases local Nusselt numbers for all blowing ratios, but this effect is reduced at higher blowing ratios. They concluded that heat transfer coefficients increase and film-cooling effectiveness values decrease with an increase in unsteady wake strength. Detailed heat transfer measurements on transonic film-cooled blade with and without NGV shock waves and wakes were made by Rigby et al. [20]. It was found that there was a significant change of film-cooling behavior on the suction surface when simulated NGV unsteady effects were introduced.

3.2. Experimental Setup

Figure 3.1 shows the experimental facility consisting of the cascade, cooling loop, and the data acquisition system. A schematic of the 5-blade cascade with optical set-up locations is shown in Figure 3.2. Two film-cooling hole orientations are tested in this study, which are axial angle and compound angle. Figures 3.3 and 3.4 show the stereo lithography (SLA) test blade with the internal coolant supply passage and the film cooling holes. The test blade had a squealer tip with a recess of 2.4% of blade span (2.84mm) while the two adjacent blades had a flat tip. The tip clearance for the test blade and the two adjacent guide blades was 1% of the blade span. Three rows of showerhead film cooling holes with a diameter of 0.65mm were provided along the leading edge of the test blade. The middle row was aligned with the stagnation line while the other two rows were placed $\pm 15^\circ$ from the stagnation line. Each showerhead row had 22 holes with a hole-to-hole spacing of 5.3mm ($s/d = 8.2$). The length to diameter ratio (L/d) for all the showerhead holes was 12.7. Four rows of laidback, fan-shaped holes were provided on the pressure side at axial locations of 1.24cm (PS1, 23 holes), 3.62cm (PS2, 22 holes), 5.01cm (PS3, 23 holes) and 6.1cm (PS4, 22 holes). Two more such rows were provided on the suction side of 0.38cm (SS1, 23 holes) and 3.56cm (SS2, 22 holes). All pressure and suction side holes were inclined 45° away from the blade surface in the mainstream flow direction as well as 45° away from the blade span. The lateral diffusion angle of the holes was 10° from the hole centerline and the forward expansion angle was 10° . The metering section of the hole had a diameter of 0.65mm, producing L/d ratio equal to 4.75. The total L/d of the hole was 9 and the expansion ratio (ratio of the exit

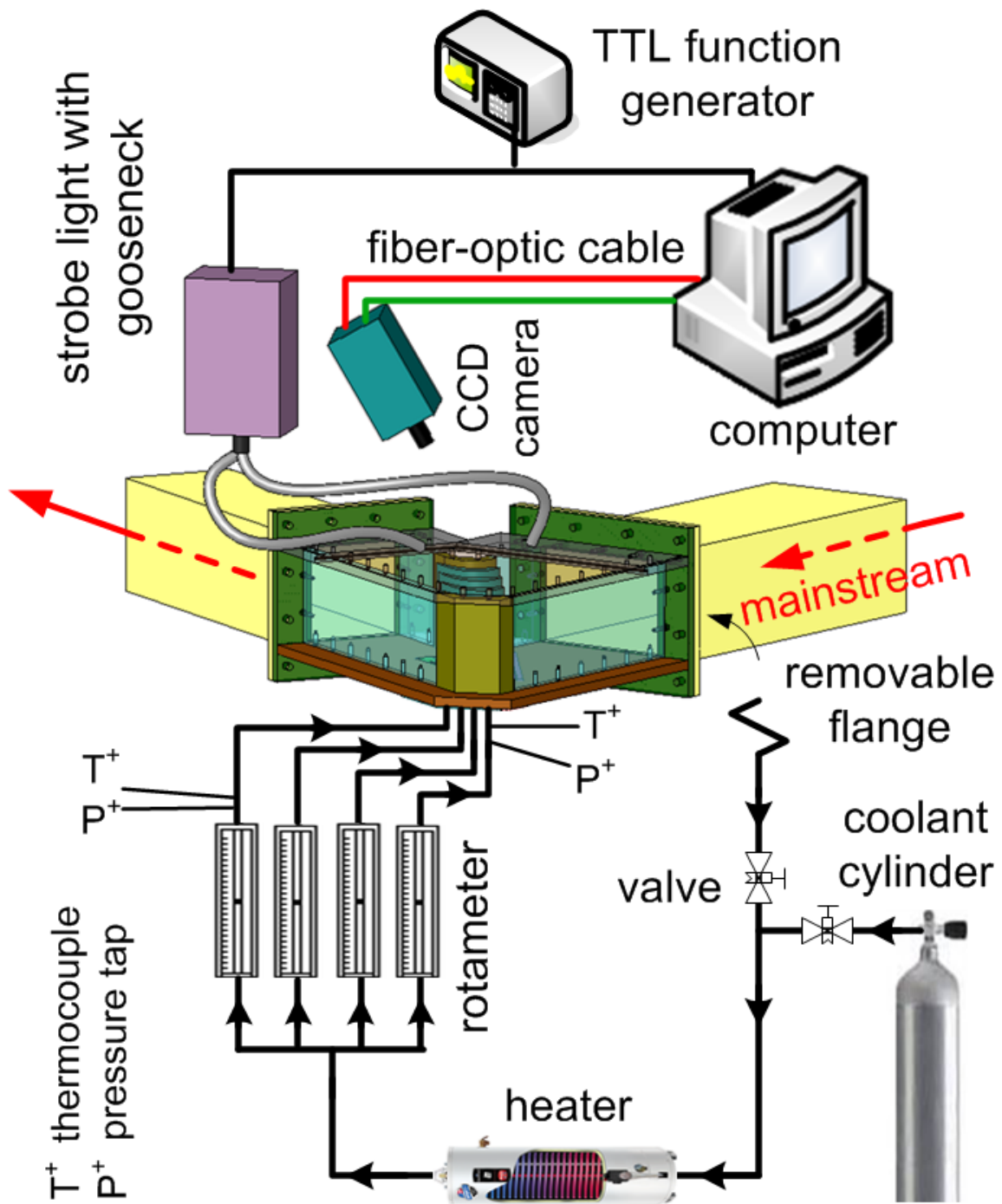
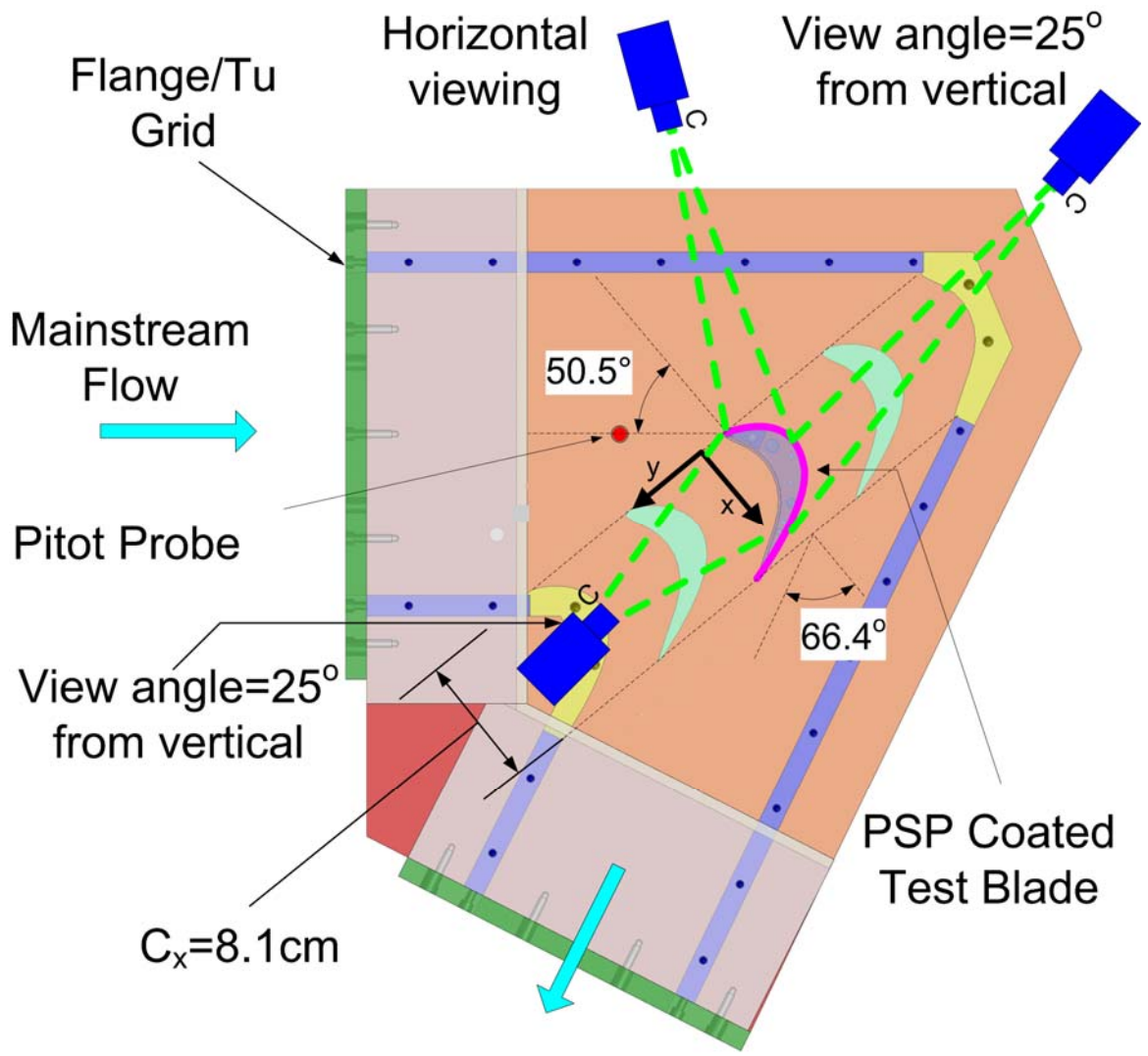


Figure 3.1 Schematic of experimental facility



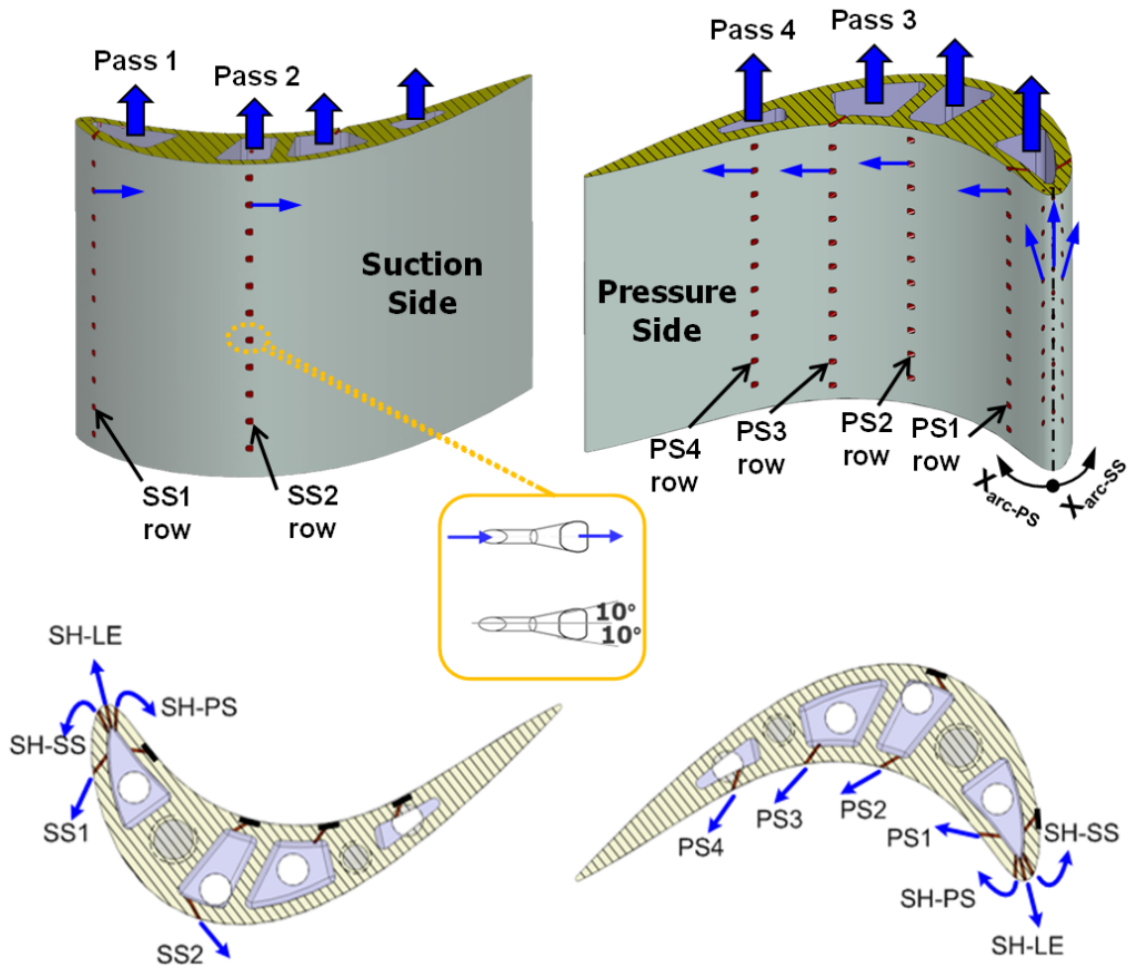


Figure 3.3 Details of the test blade (Axial shaped hole)

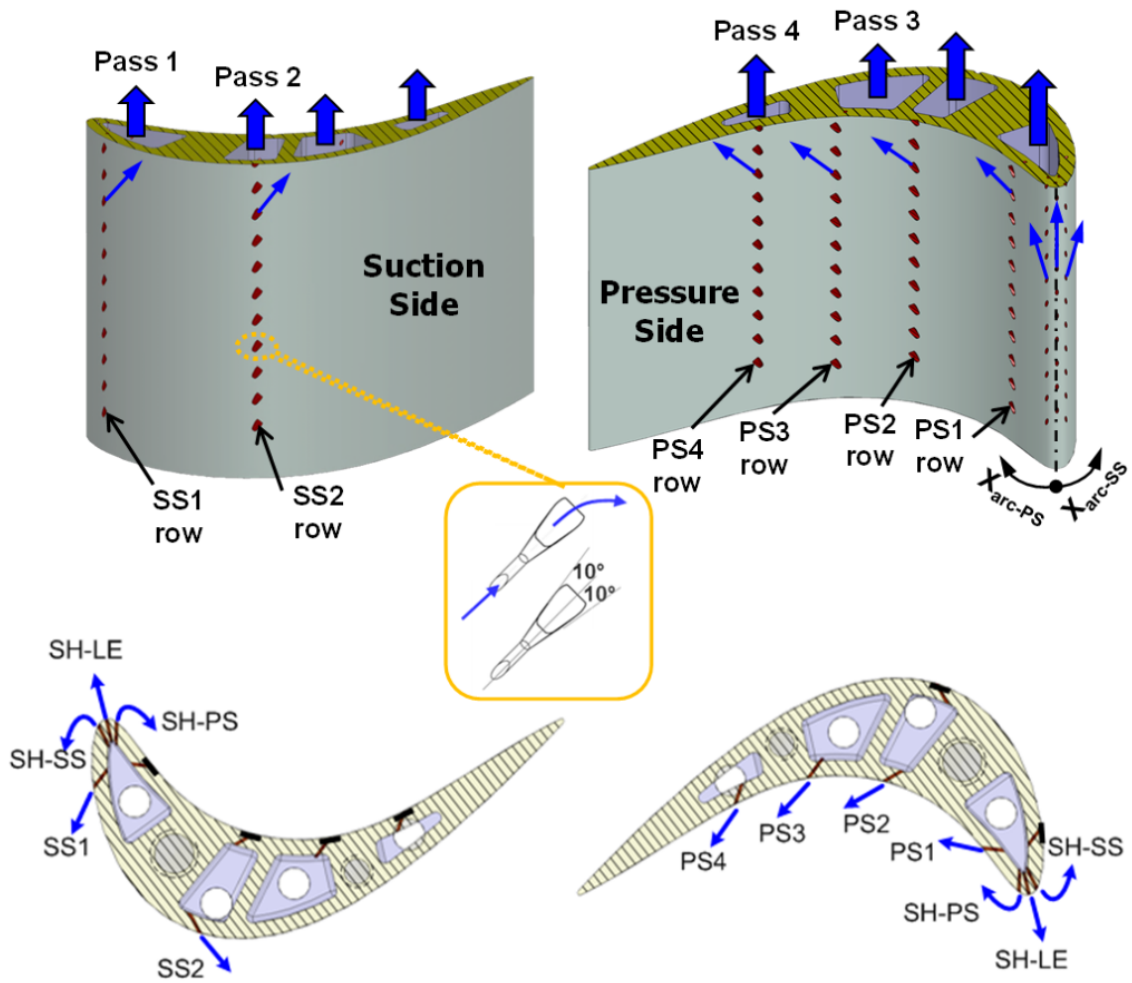


Figure 3.4 Details of the test blade (Compound shaped hole)

break-out area to the inlet cross-section area) was equal to 11. Coolant was supplied via 4 cavities, each cavity flow controlled by a rotameter. The first cavity near the leading edge was designed to supply coolant to the showerhead film cooling holes as well as rows PS1 and SS1. The second cavity was designed to supply coolant to rows PS2 and SS2. The remaining two cavities supplied coolant to rows PS3 and PS4, respectively. The cavity cross-sections were modeled similar to the internal cooling passages in turbine blades with coolant injection from the blade hub.

The mainstream air is supplied by a centrifugal compressor that could deliver a volume flow rate up to $6.2\text{m}^3/\text{s}$. The volume flow rate is regulated by a frequency controller having an operational range of 0 to 60 Hz. The cascade inlet and exit velocities are set to be 96m/s and 156m/s corresponding to inlet and exit Mach numbers of 0.27 and 0.44, respectively. The Reynolds number based on the axial chord length and exit velocity is 750,000 and the overall pressure ratio (P_t/P) is 1.14 (where P_t is inlet total pressure and P is exit static pressure). Some of important dimensions of the cascade and mainstream flow conditions are listed in Table 3.1. A total of 6 sets of experiments are performed to study the effects of blowing ratio (M), density ratio (DR), and freestream turbulence intensity (Tu) on blade film-cooling effectiveness. Three average blowing ratios – 1.0, 1.5, and 2.0 are selected for the tests. Summary of experimental conditions are shown in Table 3.2.

Three different average blowing ratios were selected – 1.0, 1.5 and 2.0. The amount of coolant supplied to each of the four cavities to attain a desired average blowing ratio was calculated using the equation:

$$\dot{m}_c = \sum_{r=1}^n M [m_m'']_r [A_c]_r \quad (7)$$

where M is the average blowing ratio, r is the coolant hole row in a cavity, n is the number of rows in a cavity, m_m'' is the mainstream mass flux at row r , and A_c is the total area of all the coolant holes at row r . The mainstream mass flux at a given row location was calculated from the total pressure measured upstream of the test blade and static pressure obtained via surface taps at 50% blade span height.

Table 3.1 Cascade geometry and mainstream flow conditions for blade span film-cooling

Conditions of Mainstream Flow			
Inlet Mach No.	0.27	Inlet Reynolds No.	465,000
Exit Mach No.	0.44	Exit Reynolds No.	750,000
Pressure ratio (P_t/P)		1.14	
Boundary layer thickness (cm)		2.5 and 0.5	
Average turbulence intensity		4.2% and 10.5%	
Integral length scale/ C_x		0.72 and 0.07	
Linear Cascade Geometry			
Blade height (cm)	12.64	Inlet area (cm ²)	249
Axial chord length (cm)	8.13	Exit area (cm ²)	164
Pitch (cm)		7.69	
Total turning angle (°)		116.9	
Blade height (cm)		12.64	
Axial chord length (cm)		8.13	

**Table 3.2 Summary of experimental conditions for
blade span film-cooling**

Expt. #	M	DR	Tu (%)
1	1.0	2.0	10.5
2	2.0	2.0	10.5
3	1.5	2.0	10.5
4	1.5	1.5	10.5
5	1.5	1.0	10.5
6	1.5	2.0	4.2

3.3. Results and Discussion

3.3.1. Effect of Blowing Ratio

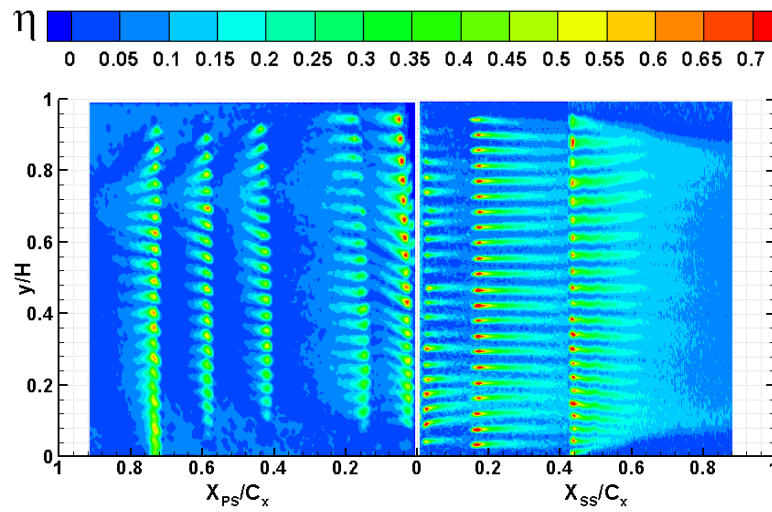
Cooling air used in film-cooling is extracted from the compressor stage and pass through the airfoils. However, discharge air from the compressor causes a penalty on engine performance. Blowing ratio is parameter, which quantifies the amount of coolant used in film-cooling. It is defined as a mass flux ratio between coolant and mainstream.

Figures 3.5 to 3.8 show the effectiveness distribution and spanwise average effectiveness as a function of blowing ratio with axial shaped hole and compound shaped hole, respectively. In the tests, the density ratio and the freestream turbulence intensity are fixed at 2.0 and 10.5%, respectively; the blowing ratio varies from 1.0 to 2.0. It can be seen that the film-cooling effectiveness increases with the blowing ratio for pressure side coolant injection. Jet lift-off is not observed even for the highest blowing ratio $M=2.0$. Improvement in film coverage is found on the suction side of the blade as well when blowing ratio is raised from 1.0 to 1.5. As blowing ratio increases to $M=2.0$, instead of enhancing film-cooling performance, thinner and shorter coolant trace with lower effectiveness level was discovered. This is indicative of more mixing of coolant and mainstream and coolant tends to left-off.

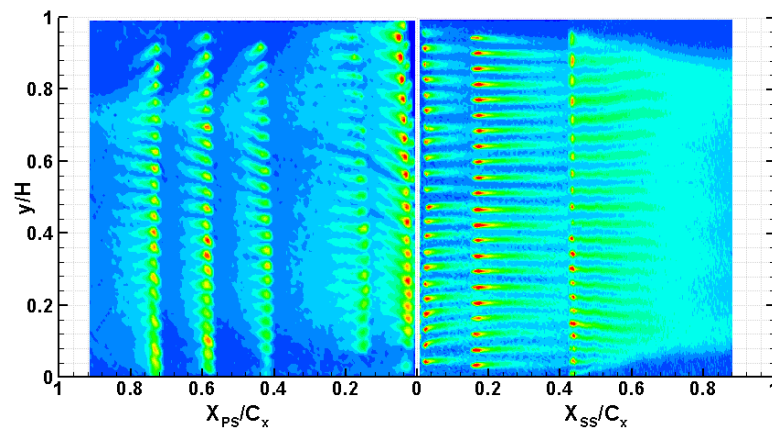
As compared to compound shaped holes in the same flow conditions, axial shaped hole produces thinner and shorter coolant traces, which is indicative of the less film-cooling coverage. With compound-angle design, the deflected jets result in wider film coverage, thus benefitting the film-cooling effectiveness.

By comparing the suction and pressure side, film-cooling trace on suction surface is much longer than that on the pressure side. The suction side convex surface produces favorable pressure gradient and flow acceleration, making it easier for coolant to stay on the surface. On the other hand, the concave surface on the pressure side, more likely causes flow separation due to the adverse pressure gradient. In general, suction side has better film-cooling coverage than the pressure surface. Therefore, the test blade has more rows of cooling holes on the pressure side than that on the suction side.

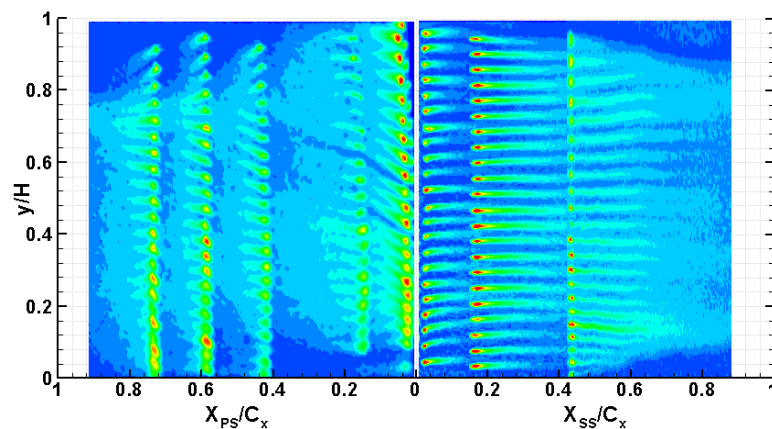
It can be seen in Figures 3.5 and 3.7 that the coolant jets on suction side are deflected by the mainstream. Starting at $X/C_x \sim 0.3$, the spiraling motion of the passage vortex near the hub surface and the tip leakage vortex draws the coolant towards the blade mid-span. It is well known that the passage vortex drifts from the pressure side leading edge towards the suction side trailing edge of the adjacent blade and climbs on to the suction surface with an up-washed motion [21, 22]. The tip leakage vortex, however, creates a down-washed motion on the pressure surface. These vortices acting on the suction surface result in a converged coolant trace toward the mid-span. On the pressure side, the corner vortices throw the coolant to the hub, leading a downward coolant tract; whereas the tip leakages draw the coolant to the blade tip. Secondary flow behavior is more obvious in low freestream turbulence intensity; see Figures 3.14(a) and 3.16(a). Similar effect on effectiveness distribution due to secondary flow is also discovered by [23, 24].



(a) $M=1.0$, $DR=2.0$, $Tu=10.5\%$



(b) $M=1.5$, $DR=2.0$, $Tu=10.5\%$



(c) $M=2.0$, $DR=2.0$, $Tu=10.5\%$

Figure 3.5 Adiabatic effectiveness distribution at three different blowing ratios (Axial shaped hole)

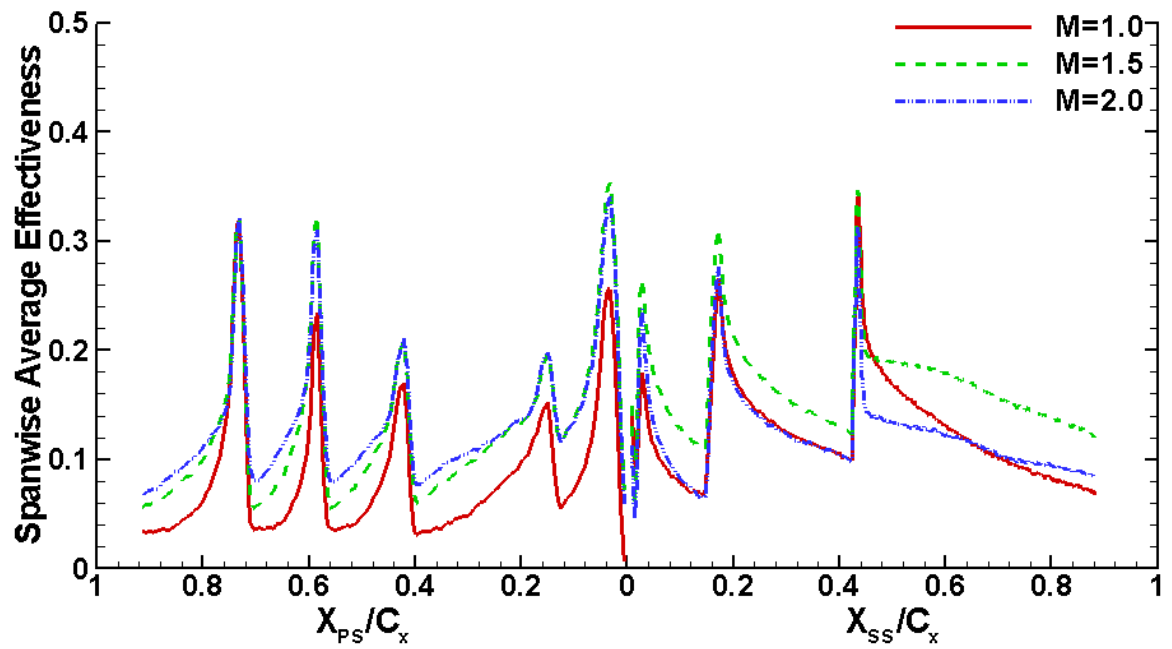
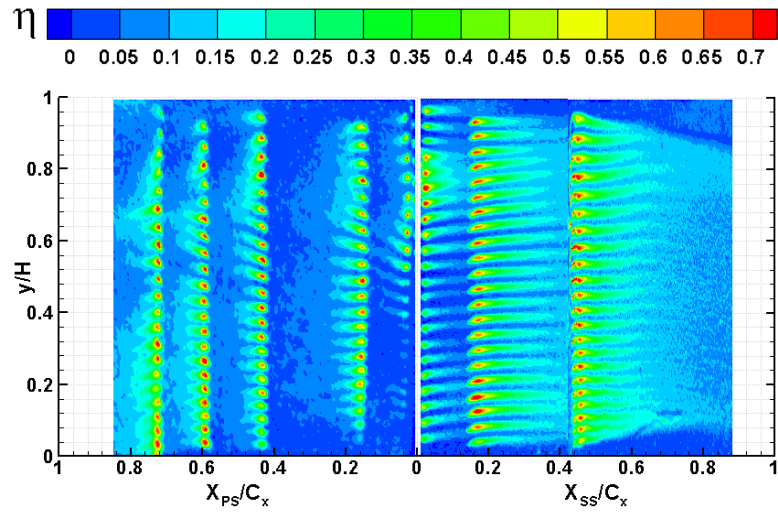
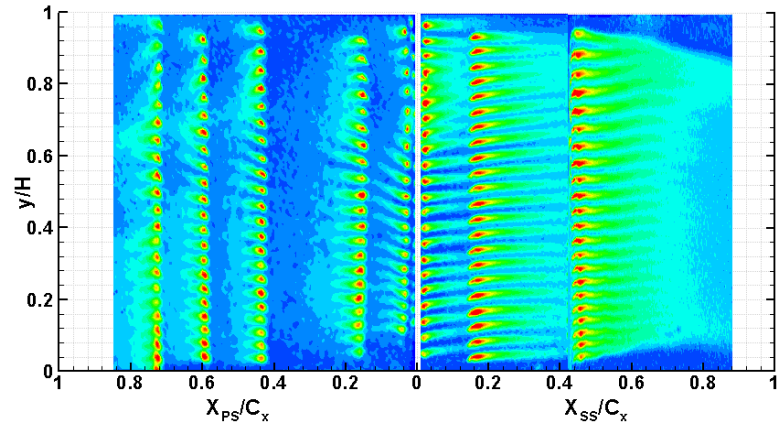


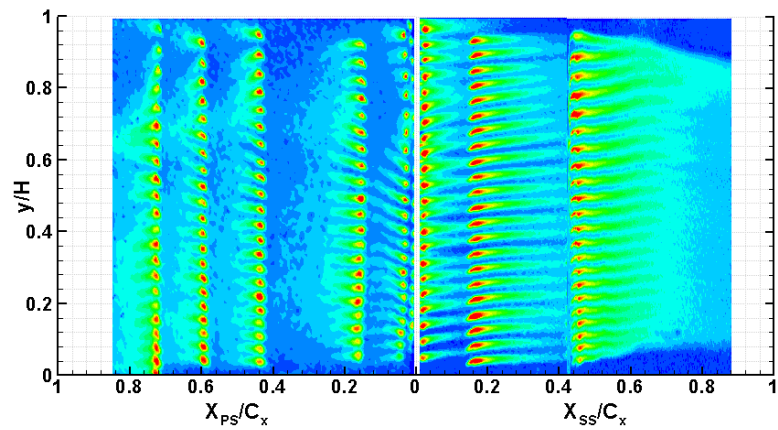
Figure 3.6 Spanwise average adiabatic effectiveness as a function of blowing ratio (Axial shaped hole)



(d) $M=1.0$, $DR=2.0$, $Tu=10.5\%$



(e) $M=1.5$, $DR=2.0$, $Tu=10.5\%$



(f) $M=2.0$, $DR=2.0$, $Tu=10.5\%$

Figure 3.7 Adiabatic effectiveness distribution at three different blowing ratios (Compound shaped hole)

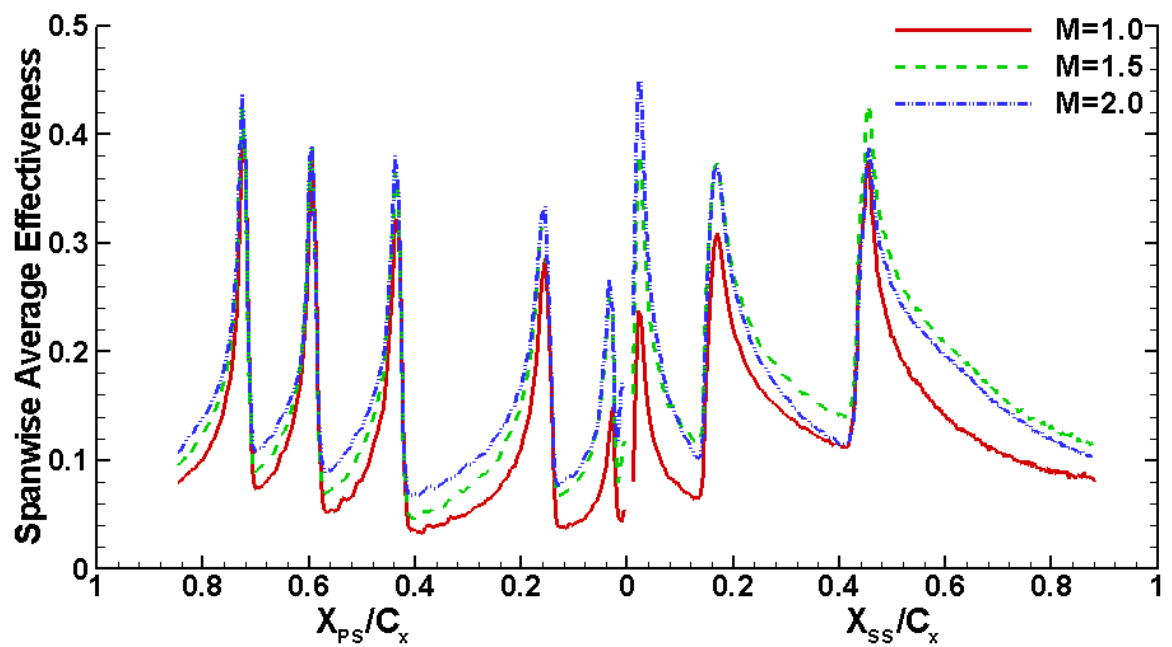


Figure 3.8 Spanwise average adiabatic effectiveness as a function of blowing ratio (Compound shaped hole)

3.3.2. Effect of Density Ratio

At engine conditions, due to the temperature difference between the coolant and mainstream, the density ratio is in the range of 1.5 to 2.0. Present study investigates the film-cooling effectiveness at three different density ratios, effectiveness contour and averaged line-plots are presented in Figure. 3.9 to 3.12. For the same blowing ratio, the coolant momentum decreases when density ratio increases. Lower coolant momentum is less susceptible to lift-off; as a result, when density ratio is increased, there is a visible improvement in effectiveness, both in terms of the trace length, width, and average effectiveness level.

Film-cooling effectiveness increases proportionally with density ratio on the suction side. Film-effectiveness continue to improve as the density ratio is raised from 1.0 to 1.5 and finally to 2.0. On the pressure side, film-cooling effectiveness also has significant improvement as density ratio increases from 1.0 to 1.5. However, there is only a minor enhancement of effectiveness when density ratio keeps rising to 2.0. The effect of curvature and secondary flow can also be seen in density ratio study.

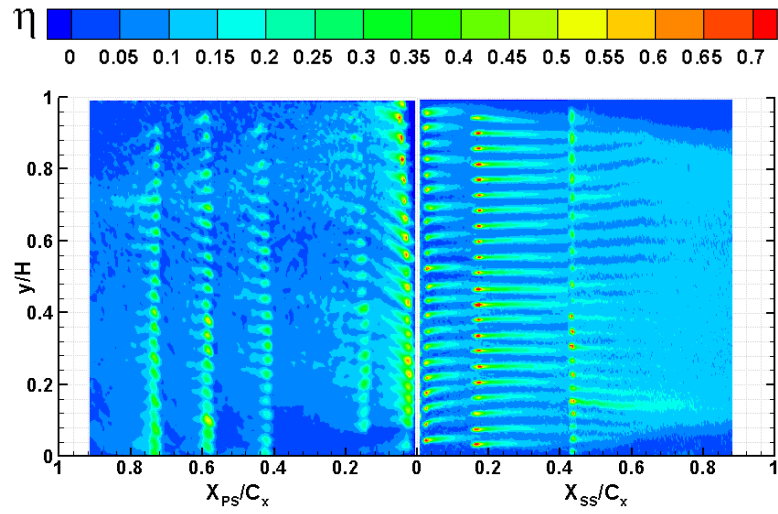
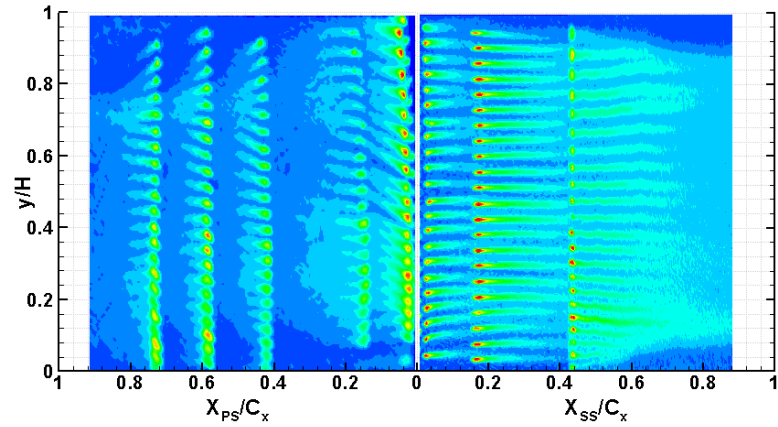
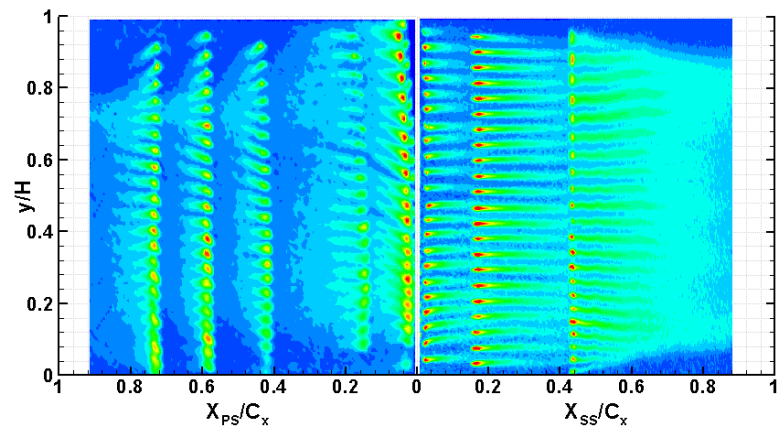
(a) $DR=1.0$, $M=1.5$, $Tu=10.5\%$ (b) $DR=1.5$, $M=1.5$, $Tu=10.5\%$ (c) $DR=2.0$, $M=1.5$, $Tu=10.5\%$

Figure 3.9 Adiabatic effectiveness distribution at three different density ratios (Axial shaped hole)

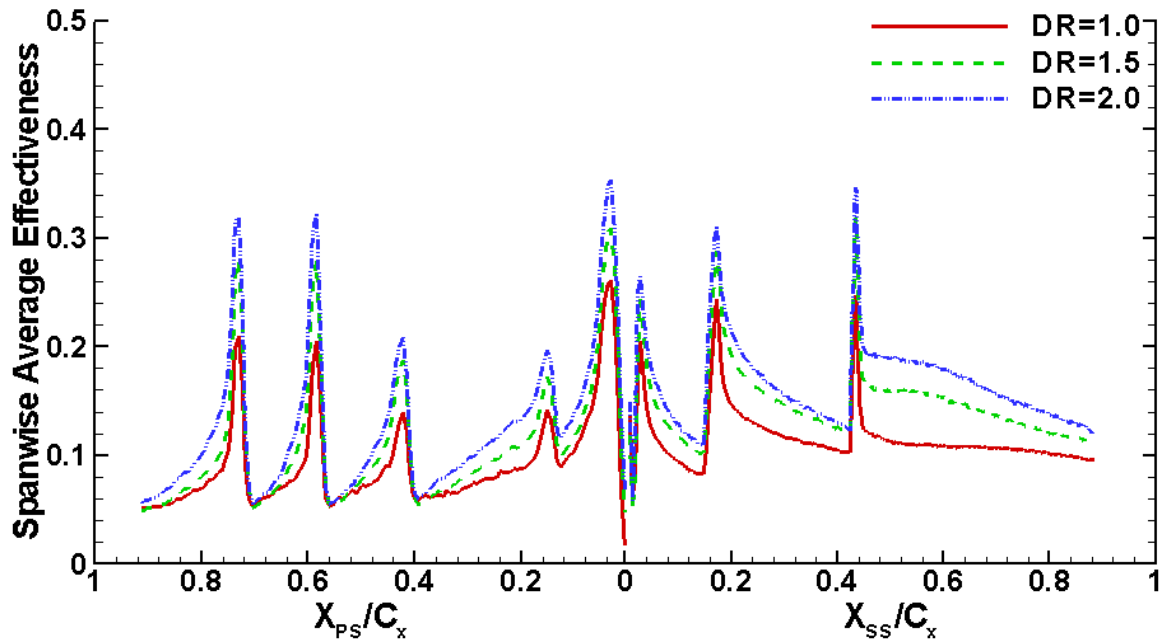
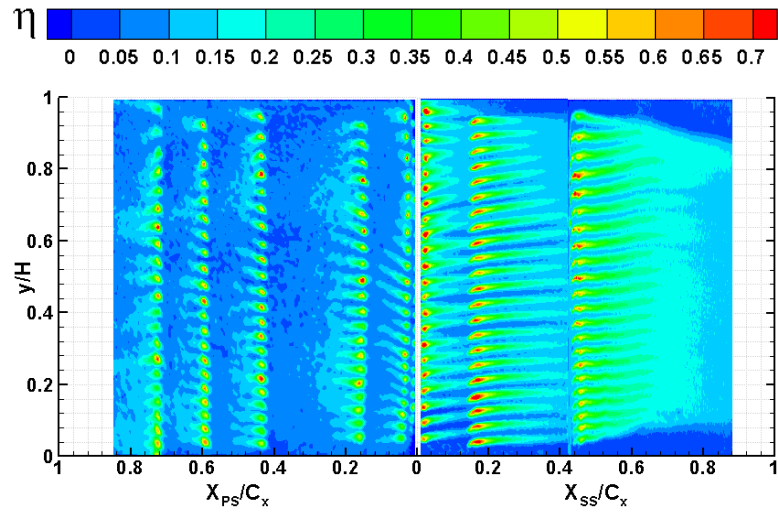
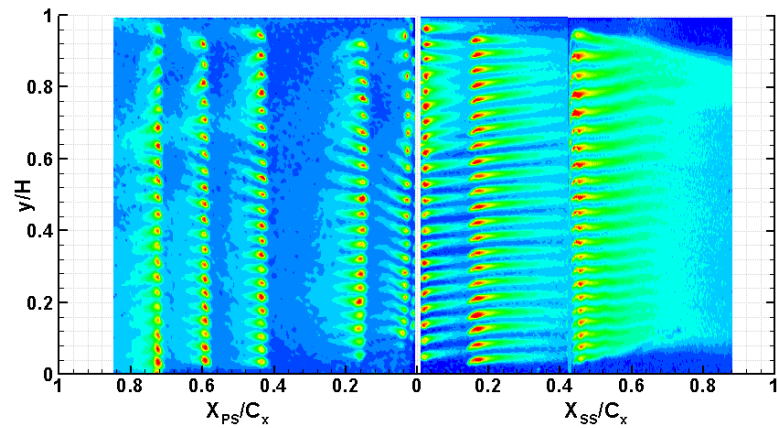


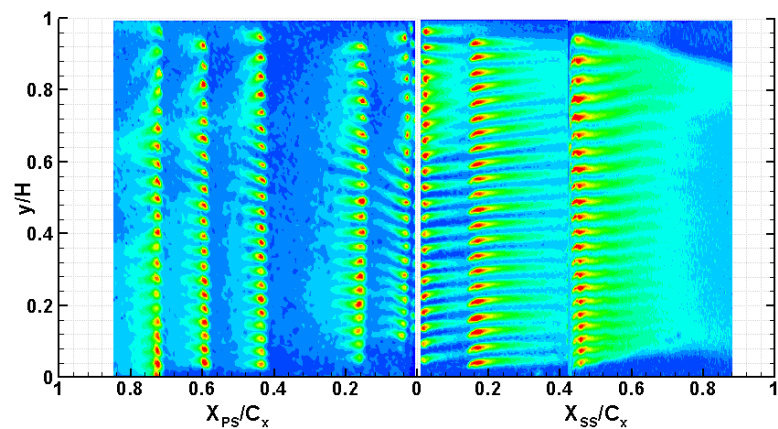
Figure 3.10 Spanwise average adiabatic effectiveness as a function of density ratio (Axial shaped hole)



(a) $DR=1.0$, $M=1.5$, $Tu=10.5\%$



(b) $DR=1.5$, $M=1.5$, $Tu=10.5\%$



(c) $DR=2.0$, $M=1.5$, $Tu=10.5\%$

Figure 3.11 Adiabatic effectiveness distribution at three different density ratios (Compound shaped hole)

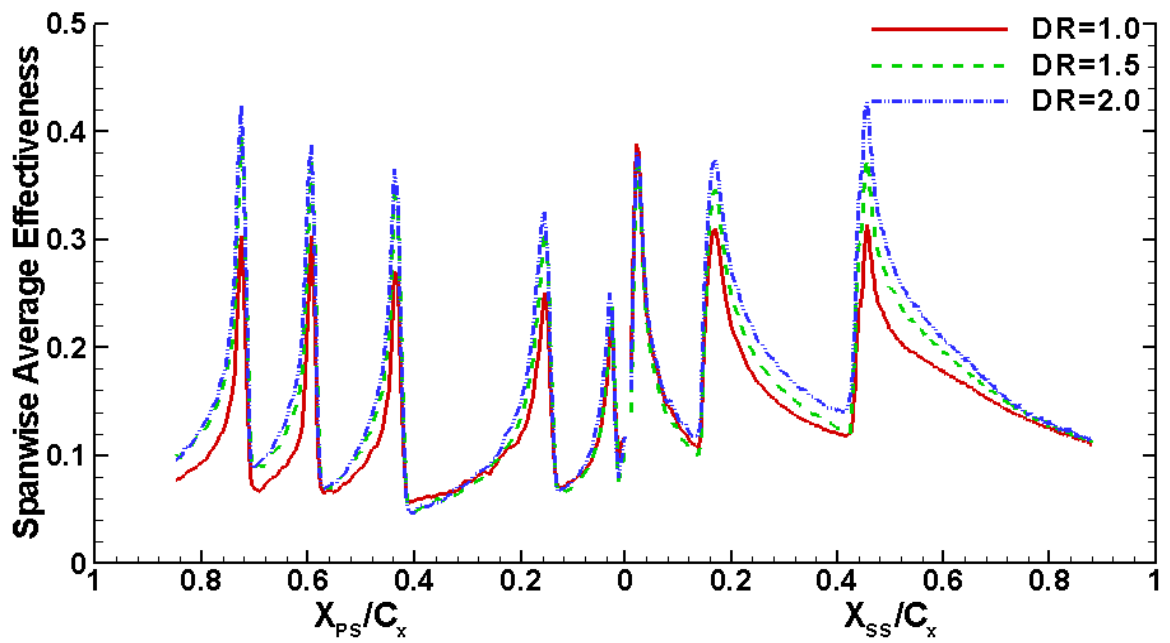
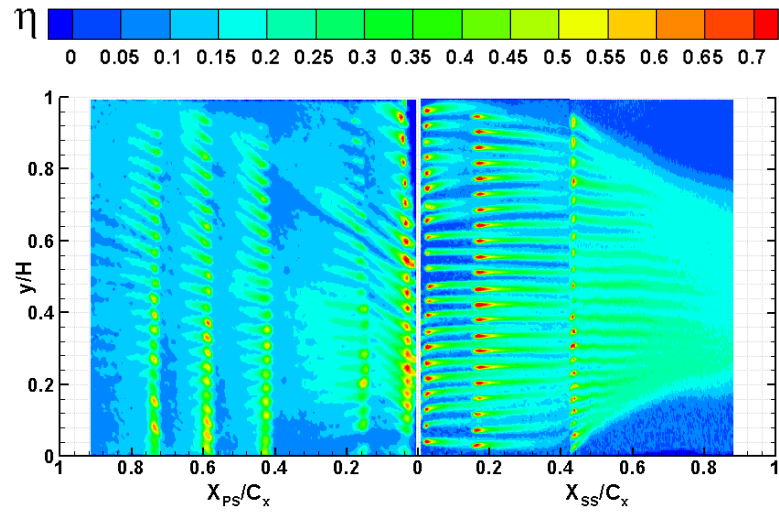


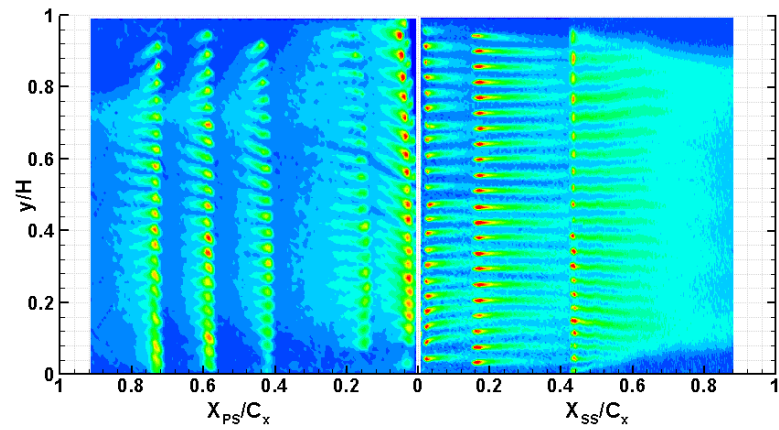
Figure 3.12 Spanwise average adiabatic effectiveness as a function of density ratio (Compound shaped hole)

3.3.3. Effect of Freestream Turbulence Intensity

High turbulence is generated by using grids upstream of the test section in a wind tunnel. To assess the influence of freestream turbulence on blade film-effectiveness, tests were performed at a low average freestream turbulence intensity of 4.2% and compared to the experiment case run at high turbulence intensity of 10.5%. Figure 3.13 to 3.16 show the resultant effectiveness distributions and spanwise average effectiveness, respectively. In general, freestream turbulence has negative effect on film-cooling effectiveness as it induces more mixing. Lower turbulence create less disturbance in the mainstream boundary layer, permitting coolant jets to progress farther and travel close to the next downstream row; thus longer and wider coolant jets appear on the pressure surface with low turbulence intensity. In the blade suction side region $X_{SS}/C_x < 0.45$, coolant jets from leading edge showerhead and first row of suction side holes decay faster at higher freestream turbulence. In the other words, coolant travels farther at the low freestream turbulence condition. However, in the region of $X_{SS}/C_x > 0.45$, unlike the upstream region, the trend in the downstream region is reversed; higher freestream turbulence produces higher effectiveness. Higher turbulence eddies play a positive role downstream of second row of suction side film-cooling hole. The passage vortices sweep less coolant away from the top and bottom edges of the blade towards the mid-span. Schmidt and Bogards [25] and Drost et al. [26] observed similar trends for momentum flux ratios greater than 0.9 on a flat plate.



(a) $Tu=4.2\%$, $M=1.5$, $DR=2.0$



(b) $Tu=10.5\%$, $M=1.5$, $DR=2.0$

Figure 3.13 Adiabatic effectiveness distribution at two different freestream turbulence intensities (Axial shaped hole)

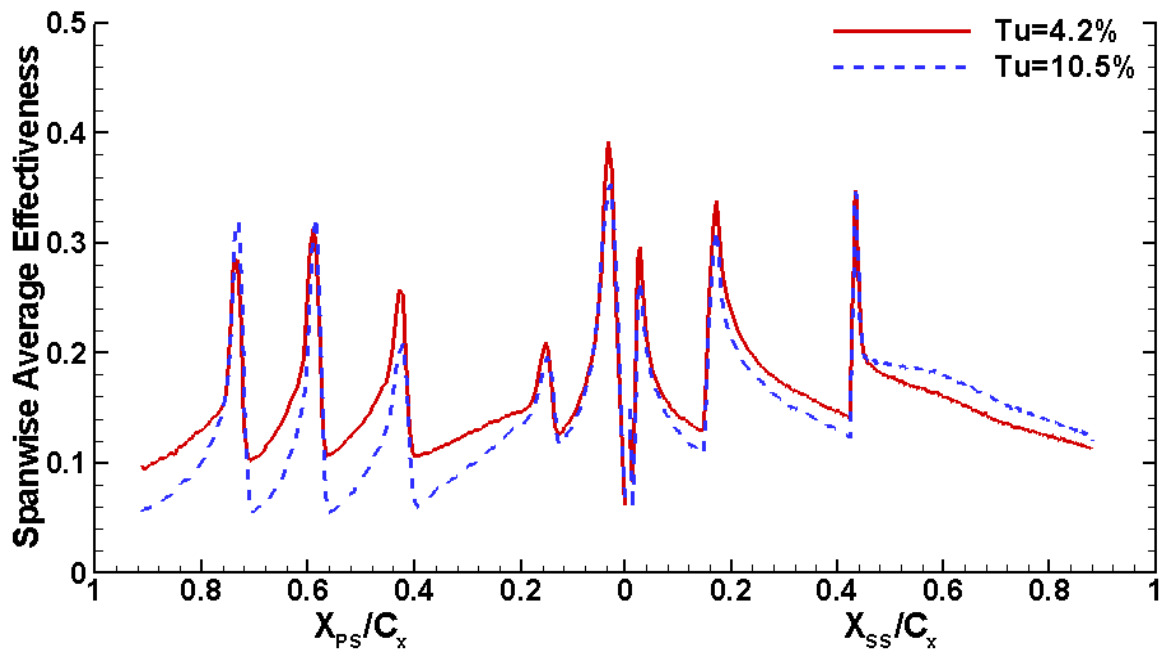
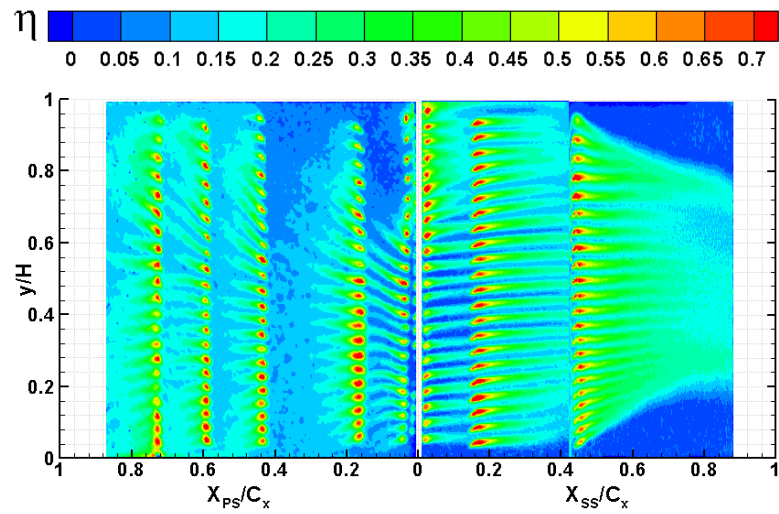
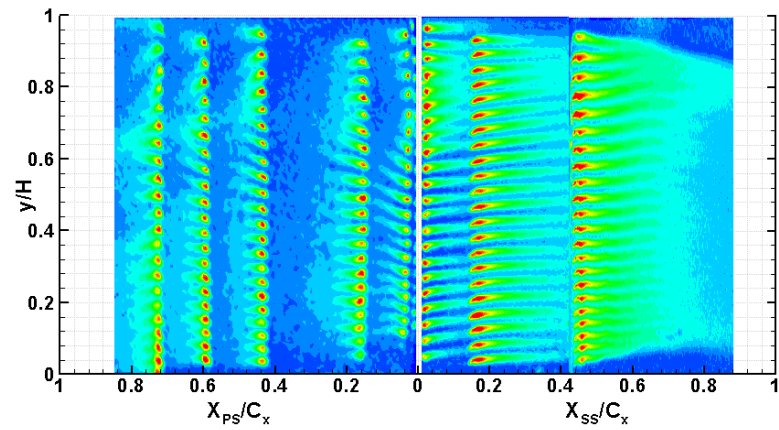


Figure 3.14 Spanwise average adiabatic effectiveness as a function of freestream turbulence intensity (Axial shaped hole)



(a) $Tu=4.2\%$, $M=1.5$, $DR=2.0$



(b) $Tu=10.5\%$, $M=1.5$, $DR=2.0$

Figure 3.15 Adiabatic effectiveness distribution at two different freestream turbulence intensities (Compound shaped hole)

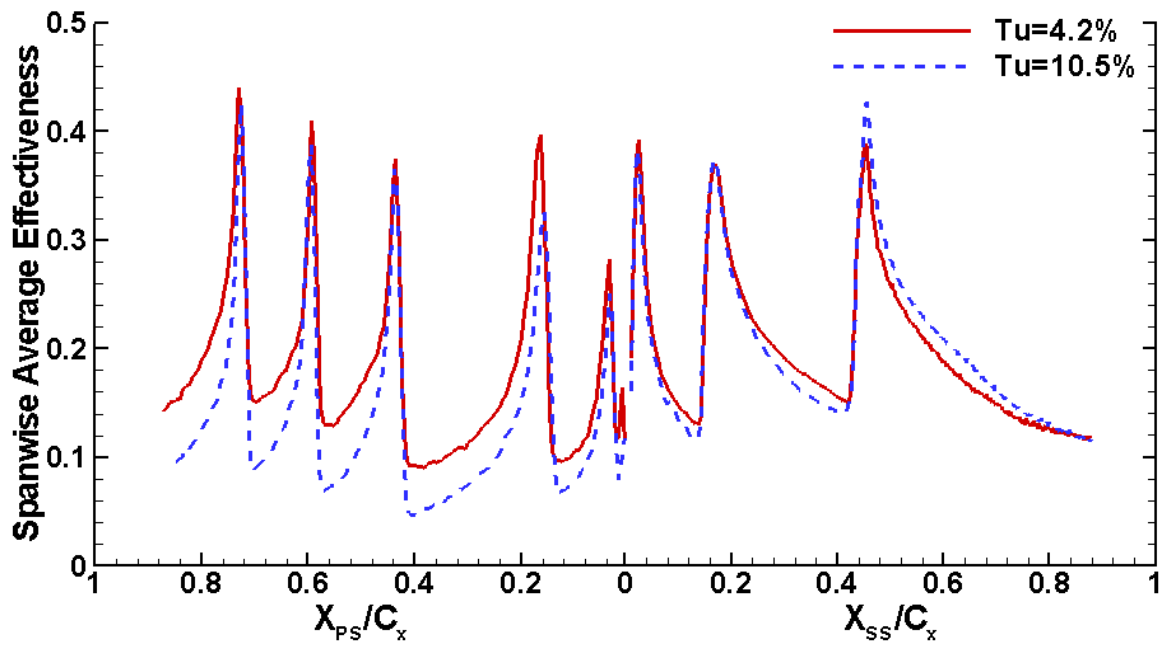


Figure 3.16 Spanwise average adiabatic effectiveness as a function of freestream turbulence intensity (Compound shaped hole)

3.3.4. Effect of Momentum Flux Ratio

The phenomenon of film cooling jet lift-off from the blade surface is understood to be governed by the ratio of coolant momentum flux to the mainstream momentum flux.

The momentum flux ratio (I) is defined as:

$$I = \frac{\rho_c V_c^2}{\rho_\infty V_\infty^2} = \frac{(\rho_c V_c)^2 / \rho_c}{(\rho_\infty V_\infty)^2 / \rho_\infty} = \frac{M^2}{DR} \quad (8)$$

Data for the present research are carefully extracted at a distance $X/D=15$ downstream from SS2 row in order to compare performance of the present blade geometry to available literature studies. Ethridge et al. [27] studied the vane suction side with 50° injection angle and strong mainstream acceleration at the point of injection. Narzary et al. [24] used the same facility as the current study to investigate film-cooling effectiveness on a gas turbine blade with compound cylindrical holes and compound-angle shaped holes, respectively. In Figure 3.17, peak effectiveness and optimum momentum flux ratio are affected by film-cooling hole geometry. Compound shaped hole has the greatest optimum momentum flux ratio, followed by axial shaped hole, compound cylindrical hole, and axial cylindrical hole. With expanded exit area (i.e., shaped hole), effectiveness peaks at higher momentum flux ratio due to the reduction of coolant jet momentum. In the other words, coolant jets are able to stay close to the surface even with large amount of coolant supply. The compound angle design makes the coolant jets spread out more laterally after deflected by the mainstream. Hence it results in relatively higher effectiveness level. In present study, data of lighter density ratio (i.e., $DR=1.5$ and 1.0) deviate from the correlation curve, which indicate that the effectiveness does not

correlate well with momentum flux ratio, although it is defined to study the combinational effect of blowing and density ratio.

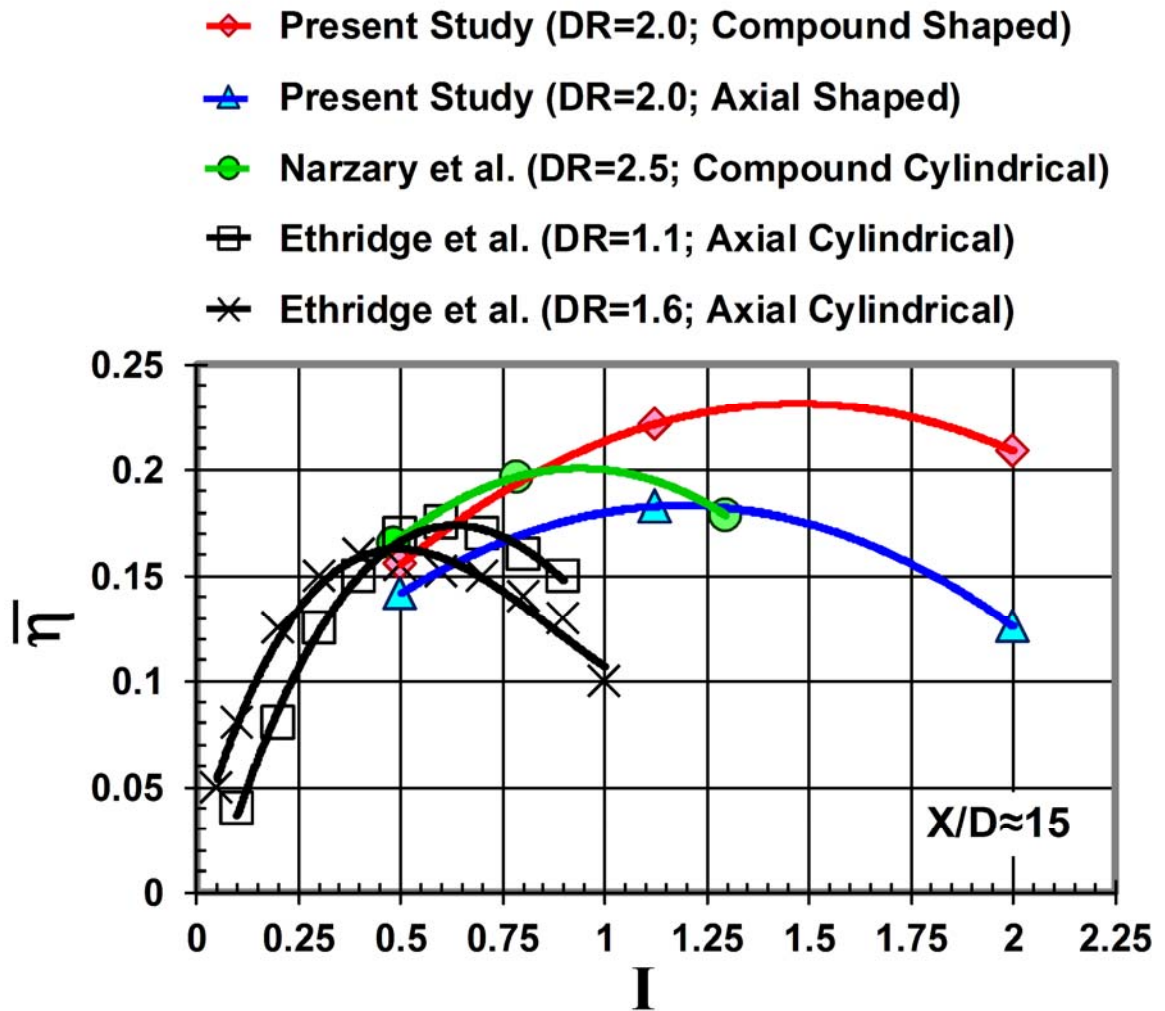


Figure 3.17 Comparison of laterally-average effectiveness

3.4. Conclusions

The present study uses PSP technique and transient liquid crystal method to measure adiabatic film-cooling effectiveness and heat transfer coefficient. The effects of blowing ratio, density ratio, freestream turbulence intensity, and momentum flux ratio are examined. Foreign gases are used to simulate density ratio heavier than air (e.g., CO₂, and mixture of Ar and SF₆). The key highlights are presented below:

- 1) Overall the compound angle provides wider film coverage and higher effectiveness level than the axial angle.
- 2) Continuous improvement of effectiveness with increasing blowing ratio can be observed on the pressure side. The effectiveness on suction side peaks at $M = 1.5$ and then diminishes when blowing ratio rises further to 2.0.
- 3) Film effectiveness on the suction side increases proportionally with density ratio. On the pressure side, significant enhancement of effectiveness is observed as density ratio increases from 1.0 to 1.5. However, only little improvement can be found when density ratio keeps rising to 2.0.
- 4) In general, freestream turbulence intensity has a detrimental effect on effectiveness. Whereas when $X_{SS}/C_x > 0.45$, film-cooling effectiveness improves with turbulence intensity.
- 5) Peak effectiveness and optimum momentum flux ratio vary with the geometry of film-cooling hole. Compound shaped hole has the greatest optimum momentum flux ratio, followed by axial shaped hole, compound cylindrical hole, and axial cylindrical hole.

- 6) Modification of endwall, blade leading edge, and film-cooling hole arrangement is considered in our next study in order to overcome the passage vortices, which sweep coolant away from the top and bottom portions near the suction side trailing edge.

4. TURBINE BLADE PLATFORM FILM-COOLING

4.1. Introduction

Many researchers have performed film-cooling on endwalls with discrete cylindrical holes. Takieshi et al. [28] obtained heat transfer and film effectiveness distributions on a vane endwall with film holes placed at three locations in the passage. The film-cooling hole configuration used by Jabbari et al. [29] consisted of discrete holes placed on the downstream half of the passage. Friedrichs [30, 31] et al. studied film-cooling effectiveness and aerodynamic loss on fully film-cooled endwall. Vogel et al. [32], and Barigozzi et al. [33] have employed shaped hole on endwall film-cooling. The above studies found that the film-cooling is strongly affected by endwall secondary flows. The cross flow transported the coolant from the pressure side to suction side of the passage. The coolant was lift off and resulted in little surface protection when film holes were located on the separation line of the secondary flow. The leading edge region of the endwall was hard to be cooled by discrete hole due to roll-up of the horseshoe vortex.

Upstream of the inlet guide vane, a gap commonly exists between the combustor and the vane endwall. A similar gap exists between the vane and the blade row. Coolant air is often expelled through these gaps or slots to prevent hot mainstream gases entering the engine cavities. This coolant air has a secondary effect of protecting the front platform region. Many researchers, including Granser and Schulenberg [34], Roy et al. [35], Burd et al. [36] and Oke et al. [37, 38], Zhang and Jaiswal [39], and Zhang and Moon [40]

have documented the characteristic of slot cooling on endwalls. These studies showed that besides cooling the hard to cool areas such as the blade leading edge, upstream slot coolant reduced the strength of secondary flows in the passage by increasing the momentum of the boundary layer of the incoming mainstream flow. Wright et al. [41] on a high-speed cascade used delta-wings to study the effect of upstream vane passage vortex on purge flow cooling. They showed the highly detrimental effect of the delta-wing generated vortex on purge flow cooling. Suryanarayanan et al. [42] investigated platform slot purge flow cooling in a three-stage turbine rotating facility. They found that the stator-rotor interaction also had a significant impact on the platform film-cooling effectiveness.

In order to provide adequate film coverage for the entire endwall or platform, a combination of both upstream slot and discrete film-cooling hole are used in real practice. Nicklas [43] measured the heat transfer coefficients and film cooling effectiveness on a Nozzle Guide Vane endwall with the combined cooling scheme. The film-cooling holes were concentrated on the entrance region of the passage, so the trailing edge region is hardly cooled. In the design of Wright et al. [44], the film holes were close to the throat region of a blade platform. The entire platform is cooled at the cost of large amount of purge flow coolant consumption. Suryanarayanan et al. [45] studied rotating platform film cooling by stator-rotor purge flow combined with discrete-hole film cooling.

Platform cooling is also influenced by the level of turbulence in the incoming mainstream flow, which could vary depending on combustor geometry. Numerous

studies have been conducted on flat plates to establish this. Kadotani and Goldstein [46], Jumper et al. [47], and Bons et al. [48] found that the film effectiveness reduces under elevated turbulence levels at low and moderate blowing ratios but improves at high blowing ratios due to coolant dispersion. In all of the above studies, the turbulence intensity was within a range of 0.3%-20.6% and coolant-to-mainstream density ratio was around 1.0. Schmidt and Bogard [25] also made similar observation with high coolant-to-mainstream density ratio of 2.0. The degree of influence of turbulence intensity on effectiveness varies with the cooling hole geometry. Colban et al. [49] presented a comparison of cylindrical and fan-shaped film-cooling holes on a vane endwall at low and high freestream turbulence levels. They observed that film-cooling effectiveness decreases with increasing turbulence level. Overall, fan-shaped holes enhanced film-cooling effectiveness by an average range of 75% over cylindrical holes.

The Turbine Heat Transfer Laboratory (THTL) at Texas A&M University has undertaken a series of study on film-cooling in their 5-blade linear cascade facility. Gao et al. [50, 51], and Narzary et al. [52] have documented the characteristics of slot cooling, discrete hole cooling, and combined cooling with various cooling hole geometries, layouts and flow conditions. The present study attempts to use PSP to investigate film-cooling performance over the full surface of a turbine platform. This study provides additional data base for the effect of coolant-to-mainstream density ratio ($DR=1$ to 2). It will provide complete information of the coolant-to density ratio effect on film-cooled platforms with two film-hole designs (cylindrical hole and shaped hole). Effects of other critical flow parameters have also been examined, including coolant blowing ratio, and

freestream turbulence intensity. Film-cooling is presented in the form of effectiveness contours and laterally average plots.

4.2. Experimental Setup

The measurements were conducted in a 5-blade linear cascade facility as shown in Figure 4.1. The inlet cross section of the test section was 19.6cm (width) x 12.7cm (height) while the exit cross section was 12.9cm (width) x 12.7cm (height). The top plate which acted as the shroud for the blades and the outer side walls of the test section were machined out of 1.27cm thick acrylic sheets for optical access. A honeycomb mesh, 7.62cm long with a cell size of 1.27cm, is put 1.78m upstream to the blade leading edge to obtain uniform velocity distribution. Flow conditions in adjacent passages of the center blade are ensured to be identical by adjusting the trailing edge tailboards for the cascade. The mainstream air is supplied by a centrifugal compressor that could deliver a volume flow rate up to 6.2m³/s. The volume flow rate is regulated by a frequency controller having an operational range of 0 to 60 Hz. The cascade inlet and exit velocities are set to be 96m/s and 156m/s corresponding to inlet and exit Mach numbers of 0.27 and 0.44, respectively. The Reynolds number based on the axial chord length and exit velocity is 750,000 and the overall pressure ratio (P_t/P) is 1.14 (where P_t is inlet total pressure and P is exit static pressure). The coolant purge flow rate is generally considered as a percentage of the mainstream mass flow rate. An earlier study [44] found that a purge flow rate of 0.5% offered very good coolant coverage compared to 0.25%. At 0.75% and beyond, the coverage was only slightly better than

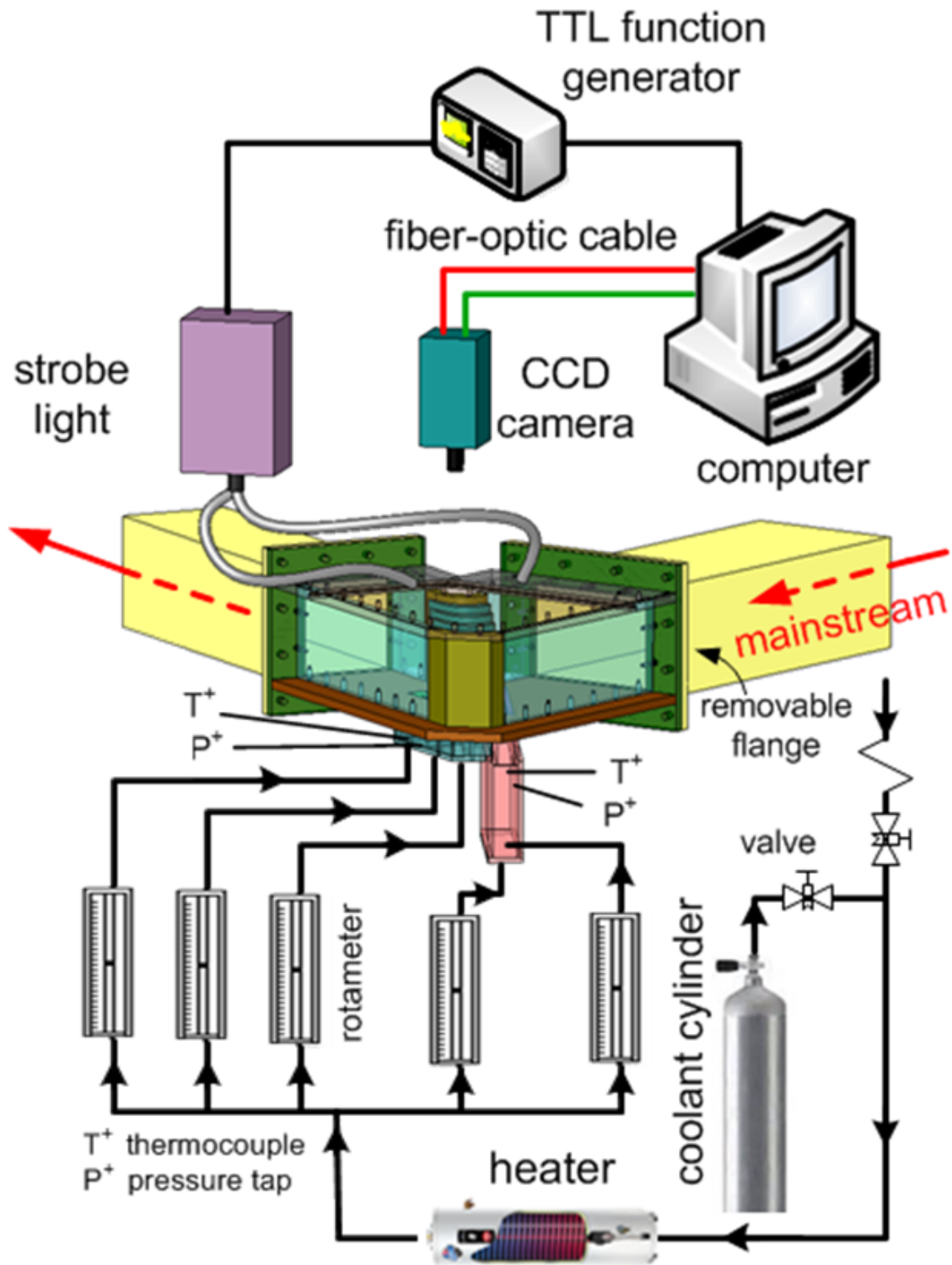


Figure 4.1 Schematic of test section facility

0.5 but the coolant consumption will substantially increase. Therefore, the mass flow ratio of 0.5% is chosen in current study.

A labyrinth-like seal, typical of a stator-rotor seal found in gas turbine engines, was used for upstream platform cooling. The seal was grown from Accura 55 resin by stereolithography (SLA) process. SLA process allows complex geometries to be created in real quick time and at a much cheaper price. Typical SLA resins have a thermal conductivity of around $0.2\text{W/m}\cdot\text{K}$. Two individual saw-toothed SLA pieces were placed side-by-side to give the seal its zigzag shape, Figure 4.2 The downstream half of the seal met the platform at an angle of 20° . The seal covered two passages of the cascade. A coolant plenum was constructed underneath the seal. Coolant entered the plenum from the two narrow sides and exited the seal after traveling through a metal screen.

Additional cooling was offered on the platform by means of discrete holes. The film-cooling holes in the current study are line-up with the freestream direction. Past studies in the open literature have confirmed that the passage cross flow sweeps the film coolant from pressure side to suction side. The jet deflection results a wider coverage area, similar to the compound angle holes on the flat plate studies. The 0.635cm thick platforms were built from the same SLA resin. Figure 4.3 shows two different hole geometries; the designs with cylindrical holes and laidback fan-shaped holes. Sixteen holes are equally distributed into two rows and more concentrated on the pressure side of the passage – one row is located along the mid-passage and the other row is offset from the pressure side of the platform surface by 6.35mm . All holes are inclined at 30° to the

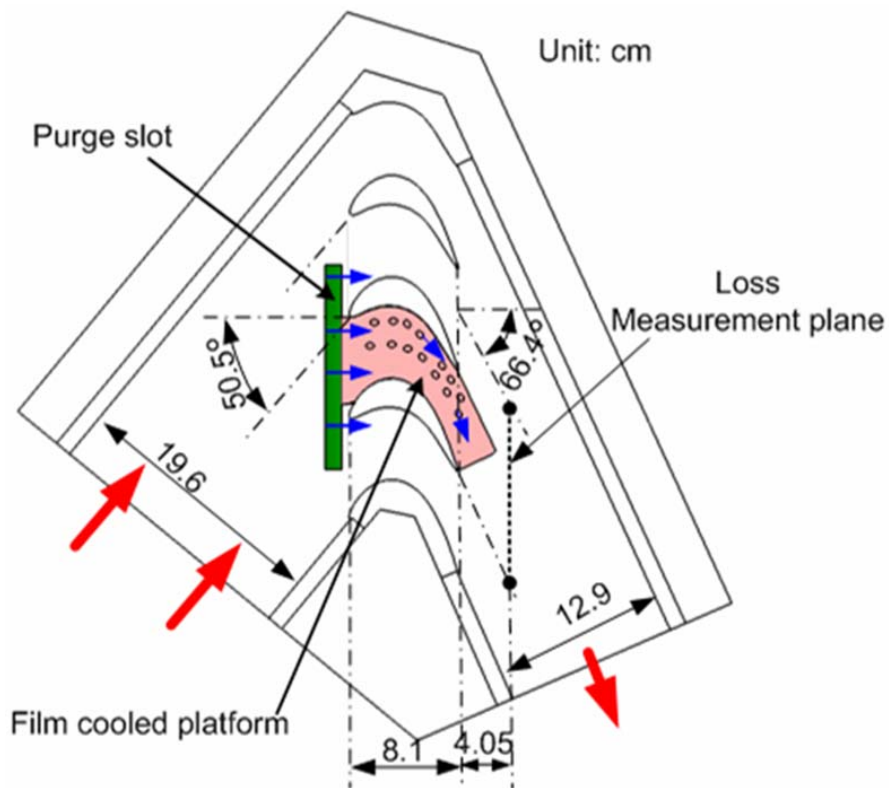


Figure 4.2 Schematic of cascade blade platform

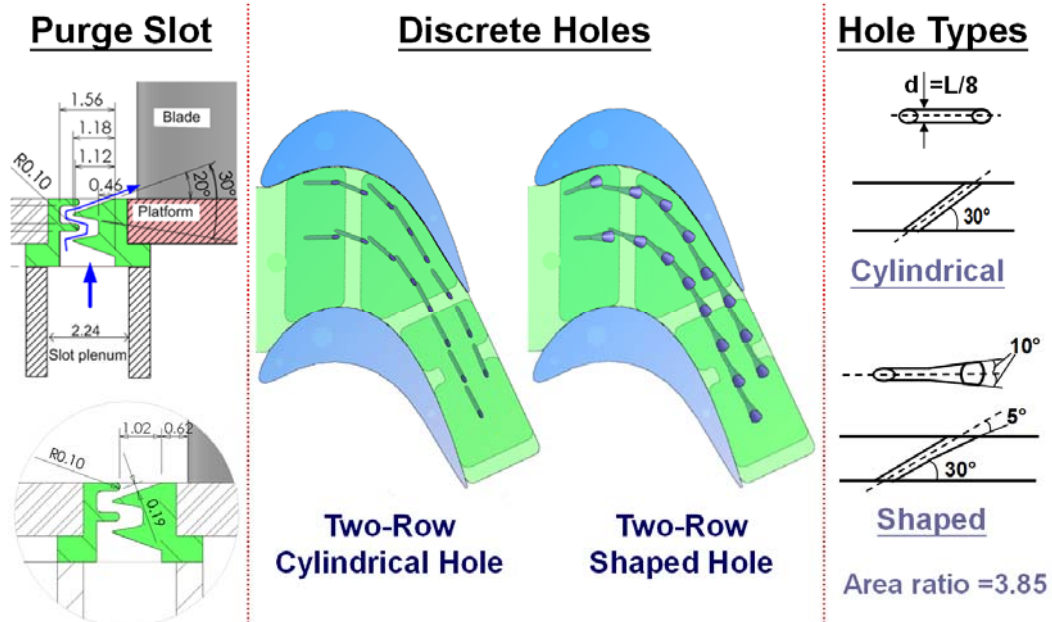


Figure 4.3 Blade platform film-cooling slot and discrete hole platform surface

and oriented along the streamwise direction with a hole-to-hole spacing around $4d$. The cylindrical holes have a diameter of 1.588mm with a hole length of $8d$. The laidback fan-shaped holes are featured with a lateral expansion of 10° from the hole axis and forward expansion 5° into the platform surface. The hole diameter in metering part of the shape holes is the same as that for the cylindrical holes. The expansion starts at $4d$, resulting in a cross section area ratio of 3.85 between the hole exit and hole inlet.

Due to the large pressure variation on the platform, it is hard to control the local blowing ratios through each cooling holes. To solve this issue, three separate coolant cavities are used. The coolant supplied to each cavity is independently controlled by its rotameter(s). Cavity I feeds hole 1 to 4; cavity II feeds hole 5 to 11; the rest holes are fed by cavity III.

A honeycomb mesh, 7.62cm long with a cell size of 1.27cm, is put 1.78m upstream to the blade leading edge to obtain uniform velocity distribution. Flow conditions in adjacent passages of the center blade are ensured to be identical by adjusting the trailing edge tailboards for the cascade. The mainstream air is supplied by a centrifugal compressor that could deliver a volume flow rate up to $6.2\text{m}^3/\text{s}$. The volume flow rate is regulated by a frequency controller having an operational range of 0 to 60 Hz. The cascade inlet and exit velocities are set to be 96m/s and 156m/s corresponding to inlet and exit Mach numbers of 0.27 and 0.44, respectively. The Reynolds number based on the axial chord length and exit velocity is 750,000 and the overall pressure ratio (P_t/P) is 1.14 (where P_t is inlet total pressure and P is exit static pressure). Some of important dimensions of the cascade and mainstream flow conditions are listed in Table 4.1. The

coolant purge flow rate is generally considered as a percentage of the mainstream mass flow rate. A total of 6 sets of experiments are performed to study the effects of blowing ratio (M), density ratio (DR), and freestream turbulence intensity (Tu) on blade film-cooling effectiveness. Three average blowing ratios – 1.0, 1.5, and 2.0 were selected for the tests. A summary of the experimental conditions is shown in Table 4.2.

Table 4.1 Cascade geometry and mainstream flow conditions for blade platform film-Cooling

Cascade Geometry			
Blade height (cm)	12.64	Inlet area (cm ²)	249
Axial chord length (cm)	8.13	Exit area (cm ²)	164
Pitch (cm)	7.69	Inlet angle (°)	50.5
Total turning angle (°)	116.9	Exit angle (°)	66.4
Mainstream Flow Conditions			
Inlet Mach No.	0.27	Inlet Reynolds No.	465,000
Exit Mach No.	0.44	Exit Reynolds No.	750,000
Pressure ratio (P _t /P)		1.14	
Boundary layer thickness (cm)		2.5 and 0.5	
Average turbulence intensity		4.2% and 10.5%	
Integral length scale/C _x		0.72 and 0.07	

Table 4.2 Summary of experimental conditions for blade platform film-cooling

Expt. #	MFR (%)	M	DR	Tu (%)
1	0.5	1.0	1.5	10.5
2	0.5	2.0	1.5	10.5
3	0.5	1.5	1.5	10.5
4	0.5	1.5	1.0	10.5
5	0.5	1.5	2.0	10.5
6	0.5	1.5	1.5	4.2

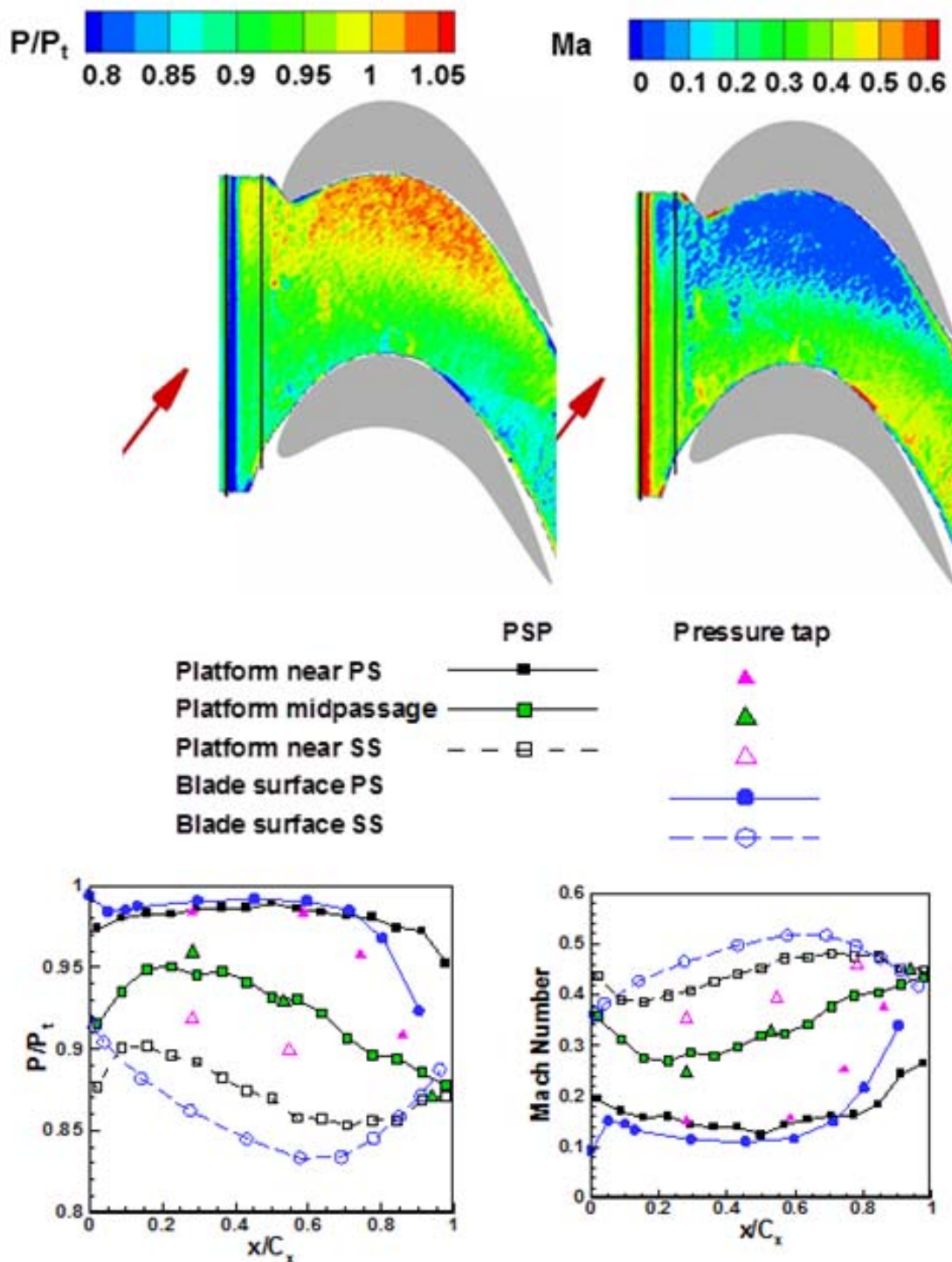
4.3. Results and Discussion

4.3.1. Pressure Measurement on Platform

The pressure and Mach number distribution on the platform are examined and shown in Figure 4.4. The pressure distribution on the platform surface is mapped using PSP and compared with static pressure data obtained by pressure taps. The match is found to be quite reasonable. It can be seen from the contour plot that the static pressure near the pressure side is higher than that near the suction side. This is the driving force of turbine work as well as the passage across flow. From the leading edge to trailing edge, the pressure gradually decreases; the mainstream flow is accelerated; Mach number increases. The outer pressure distribution is found to be highly non-uniform, which affects purge flow distribution along the slot as well as the local blowing ratio distribution from the discrete holes. From the suction side to pressure side along the purge slot, the outer pressure increases, the local coolant mass flow ratio decreases. The high outer pressure near the pressure side of the passage prohibits the coolant exiting from film cooling holes.

4.3.2. Adiabatic Film-Cooling Effectiveness

Some common features of platform film-cooling are observed regardless of hole shapes, blowing ratio and other factors. It is clear that the effectiveness distribution by purge flow is skewed with more coolant appearing from the slot end close the blade suction side, indicating the non-uniform outer pressure as stated earlier and the purge flow is swept aside by the passage cross flow. The passage vortex (conceptually shown



(a) Pressure distribution (b) Mach number distribution
 Figure 4.4 Pressure and Mach number distribution without coolant injection

by a white helix), that originates at the blade leading edge and gains in strength as it travels downstream, forms a barrier that prevents the coolant from traveling downstream. At downstream film-cooling holes, coolant is deflected to the suction side of passage by the cross flow within the passage. Due to the jet deflection, the jets from the holes offset from the pressure side are not able to impinge to the blade pressure side. Therefore, the junction area between the platform and the blade pressure side is unprotected by the film-cooling. Moreover, the horseshoe vortex (conceptually shown in black helix) also makes the junction area between the platform and the blade leading unprotected.

4.3.3. Effect of Density Ratio

The effectiveness contours plots for a range of density ratio with Configuration A and B are presented in Figures 4.5 and 4.6. Freestream turbulence, purge flow, and blowing ratio are fixed at 10.5%, 0.5%, and 1.5, respectively. For the cylindrical holes, as density ratio increases, the coolant traces are distinct and longer. The higher coolant momentum in the case of low density coolant facilitates jet detachment from the platform resulting in lower film effectiveness whereas lower coolant momentum for high density coolant keeps the jet attached to the platform producing better film-cooling coverage. Similar observation can be seen for the shaped holes, the film-cooling effectiveness elevates with density ratio. The coolant distribution immediately downstream of the slot shows no significant variation with density ratio.

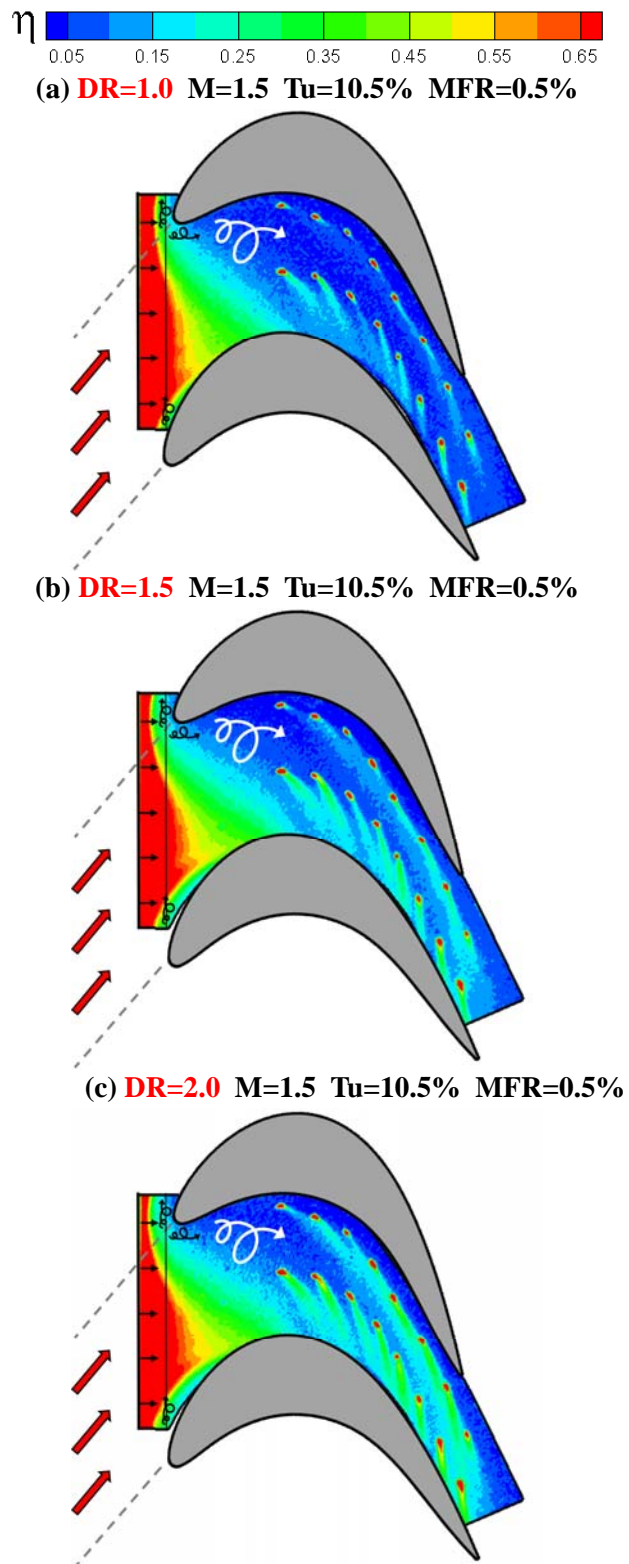
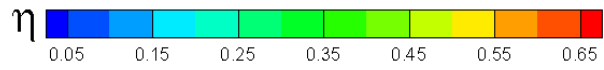
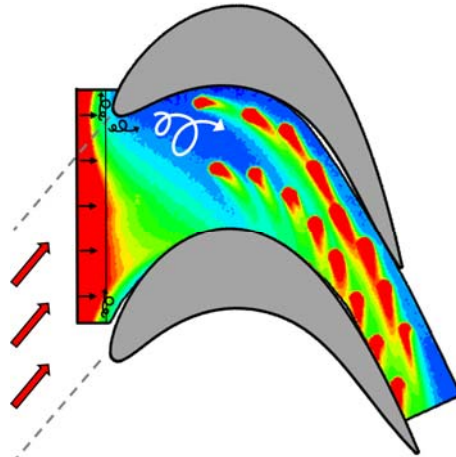


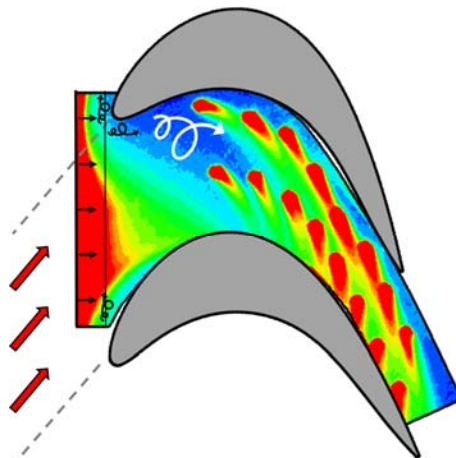
Figure 4.5 Density ratio effect on adiabatic film-cooling effectiveness for Config. A (a) DR=1.0, (b) DR=1.5, (c) DR=2.0



(a) **DR=1.0** M=1.5 Tu=10.5% MFR=0.5%



(b) **DR=1.5** M=1.5 Tu=10.5% MFR=0.5%



(c) **DR=2.0** M=1.5 Tu=10.5% MFR=0.5%

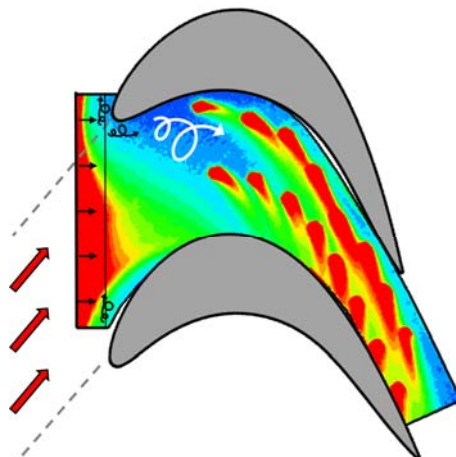


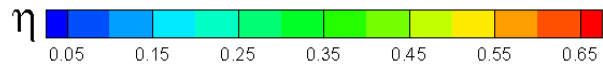
Figure 4.6 Density ratio effect on adiabatic film-cooling effectiveness for Config. B (a) DR=1.0, (b) DR=1.5, (c) DR=2.0

4.3.4. Effect of Blowing Ratio

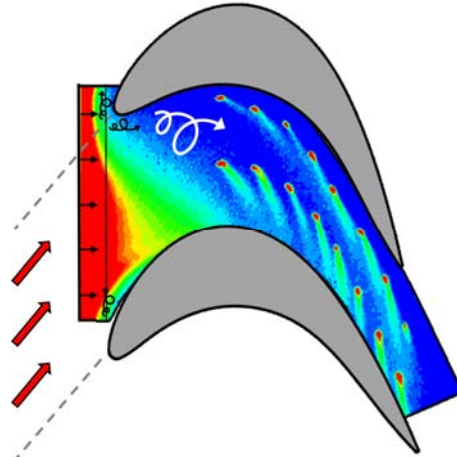
Figures 4.7 and 4.8 show the film effectiveness distributions for a range of blowing ratio with Configuration A and B. The values of purge flow rate ($MFR=0.5\%$), density ratio ($DR=1.5$), and freestream turbulence intensity ($Tu=10.5\%$) are selected to simulate engine-like flow conditions. As expected in all cases, the same purge flow delivery produced identical coolant distributions downstream of the slot. Comparing two different geometry designs, it can be seen that the shaped holes offers a larger film coverage and higher effectiveness magnitude. The best film-cooling effectiveness for cylindrical holes is obtained at $M=1.5$. Further increases of blowing ratio results in jet penetration to the mainstream and reduces the effectiveness level. For the shaped holes, the film effectiveness increases with the increases of average blowing ratio. The hole exit area is enlarged for the shaped holes and the jet momentum reduces; the coolant jet is easier to stay close to the surface. In addition, the jets from the shaped holes create wider coolant traces and accumulate at the downstream.

4.3.5. Effect of Freestream Turbulence Intensity

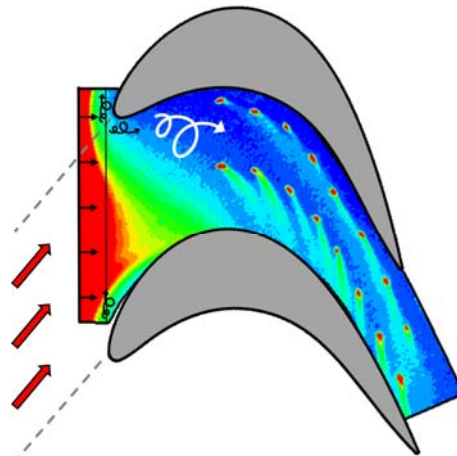
Depending on the combustor arrangement used in the industry, the turbulence intensity varies from 5% to 20% entering the turbine section. The present study performs the platform film-cooling measurements for both low freestream turbulence level ($Tu=4.2\%$) and high freestream turbulence level ($Tu=10.5\%$). The contours of film-cooling effectiveness for Configuration A and B are shown in Figures 4.9 and 4.10. It can be clearly observed from the distribution around the film-cooling holes, the coolant



(a) **M=1.0** DR=1.5 Tu=10.5% MFR=0.5%



(b) **M=1.5** DR=1.5 Tu=10.5% MFR=0.5%



(c) **M=2.0** DR=1.5 Tu=10.5% MFR=0.5%

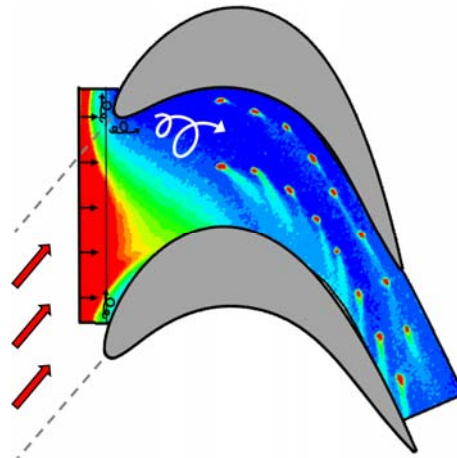
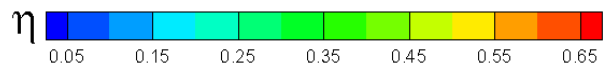
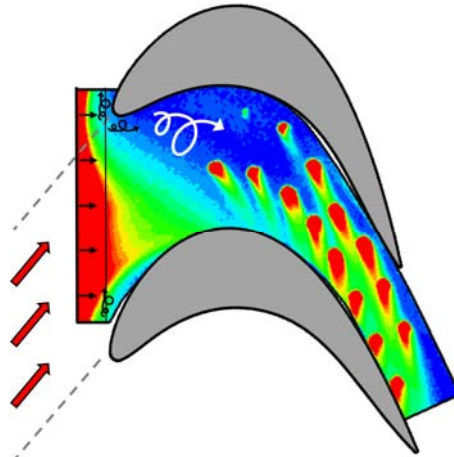


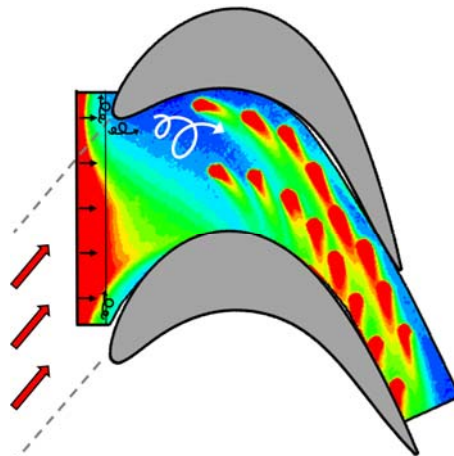
Figure 4.7 Blowing ratio effect on adiabatic film-cooling effectiveness for Config. A (a) M=1.0, (b) M=1.5, (c) M=2.0



(a) $M=1.0$ DR=1.5 Tu=10.5% MFR=0.5%



(b) $M=1.5$ DR=1.5 Tu=10.5% MFR=0.5%



(c) $M=2.0$ DR=1.5 Tu=10.5% MFR=0.5%

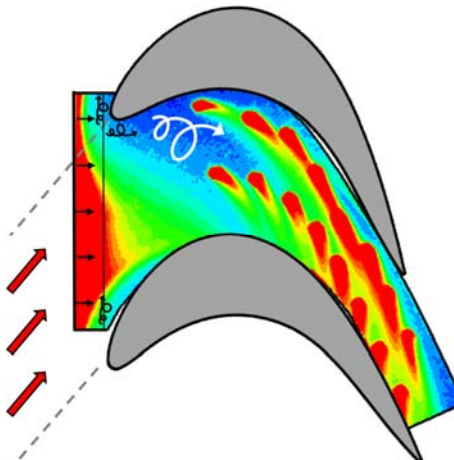


Figure 4.8 Blowing ratio effect on adiabatic film-cooling effectiveness for Config. B (a) $M=1.0$, (b) $M=1.5$, (c) $M=2.0$

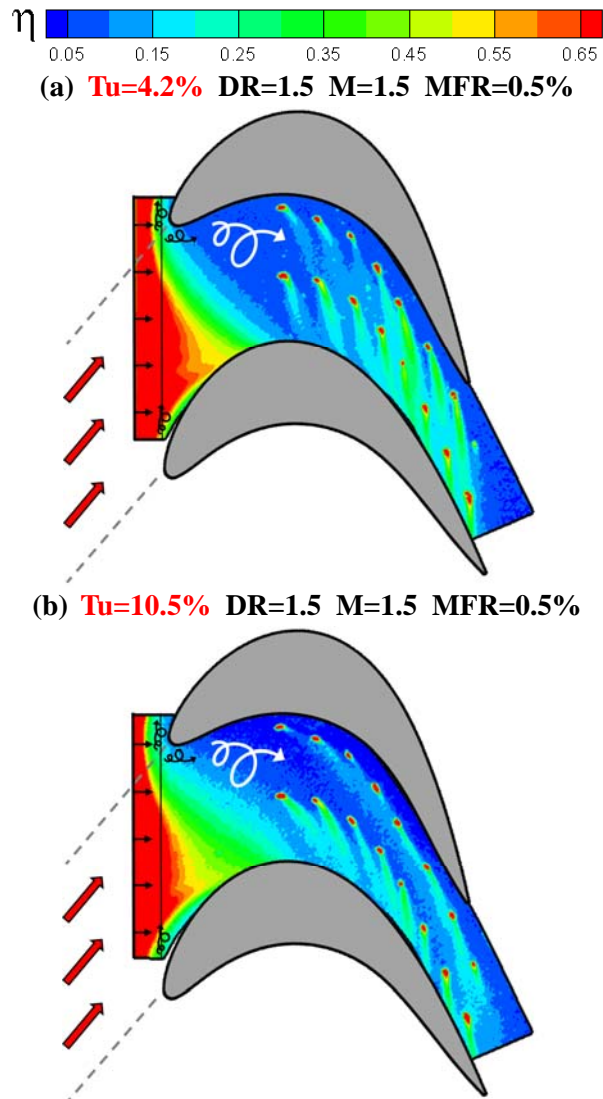


Figure 4.9 Turbulence intensity effect on adiabatic film-cooling effectiveness for Config. A
(a) Tu=4.2%, (b) Tu=10.5%

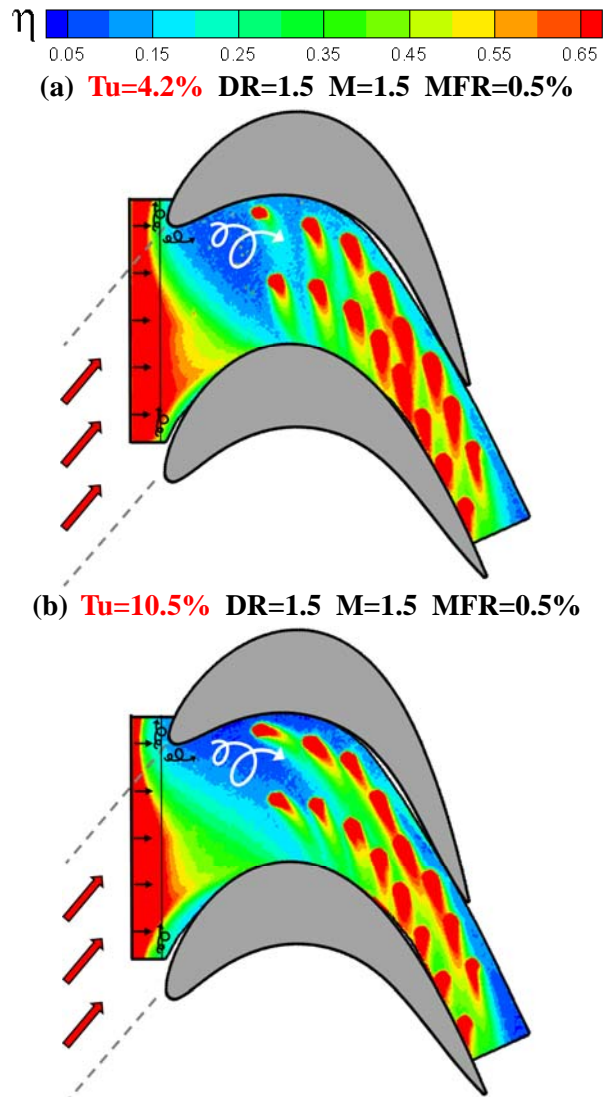


Figure 4.10 Turbulence intensity effect on adiabatic film-cooling effectiveness for Config. B
(a) Tu=4.2%, (b) Tu=10.5%

traces are longer and wider in the low turbulence case. At the elevated turbulence level, the coolant traces decay rapidly. The purge flow distribution is also affected by the level of freestream turbulence. Coolant emerges more uniformly from the slot at low turbulence. However, the purge flow can be carried further downstream and less skew at high turbulence. Generally, higher turbulence level in the mainstream indicates more mixing between the coolant and mainstream and reduces cooling performance.

4.3.6. Laterally Average Film-Cooling Effectiveness

Figures 4.11 and 4.12 show the effect of blowing ratio, density ratio, and turbulence intensity on laterally averaged film-cooling effectiveness based on two different hole configurations. The points $x/C_x=0$ and 1.0 correspond to the blade leading and trailing edges. The purge flow begins and exits the slot at $x/C_x=-0.15$ and -0.075 , respectively. It can be observed that two cooling sources are clearly depicted on the plots: A purge flow cooling peaks at $x/C_x=-0.1$ with magnitude of 0.95; film-cooling through discrete film-cooling holes after $x/C_x=0.35$. Several peaks between $x/C_x=0.35$ and 1.0 indicates numbers of pairs of holes between the blade leading and trailing edges.

In Figures 4.11(a) and 4.12(a), it appears that unlike the discrete hole cooling, the purge flow cooling does not have a substantial impact by density ratio. On both cylindrical holes and shaped holes, the effectiveness level of discrete hole cooling increases with density ratio. For the cylindrical holes, the effectiveness enhancement due to heavier coolant is proportional. On the other hand, the improvement of effectiveness for the shaped holes becomes less significant as compared to the cylindrical holes. For

the purge flow cooling, since the effectiveness level is already very high (peaks at about 0.95 over the slot), the advantage of heavier density coolant is not obvious.

Similar to contour plots, Figure 4.11(b), for cylindrical holes, the best film-cooling performance occurs at a blowing ratio of 1.5. The effectiveness levels increase about 40% when blowing ratio is increased from 1.0 to 1.5. With further increase to 2.0, the effectiveness levels drop sharply, even dropping below the level at $M=1.0$. In Figure 4.12(b), for shaped holes, the effectiveness levels increase at most 30% when blowing ratio is increased from 1.0 to 1.5. With further increases to 2.0, the enhancement of effectiveness levels is not significant. The upstream purge flow for both configurations produces nearly identical effectiveness levels since the mass flow rates are the same.

As seen earlier in the contour plots, Figures 4.11(c) and 4.12(c) show that lower freestream turbulence leads to higher effectiveness levels throughout most of the platform, except at the downstream of the slot where the high turbulence flow display higher effectiveness. Close to the blade trailing edge, for cylindrical holes, the effectiveness levels with the low turbulence case are at most 40% higher than that with the high turbulence case. The shaped holes follow the same pattern but with smaller improvement in effectiveness.

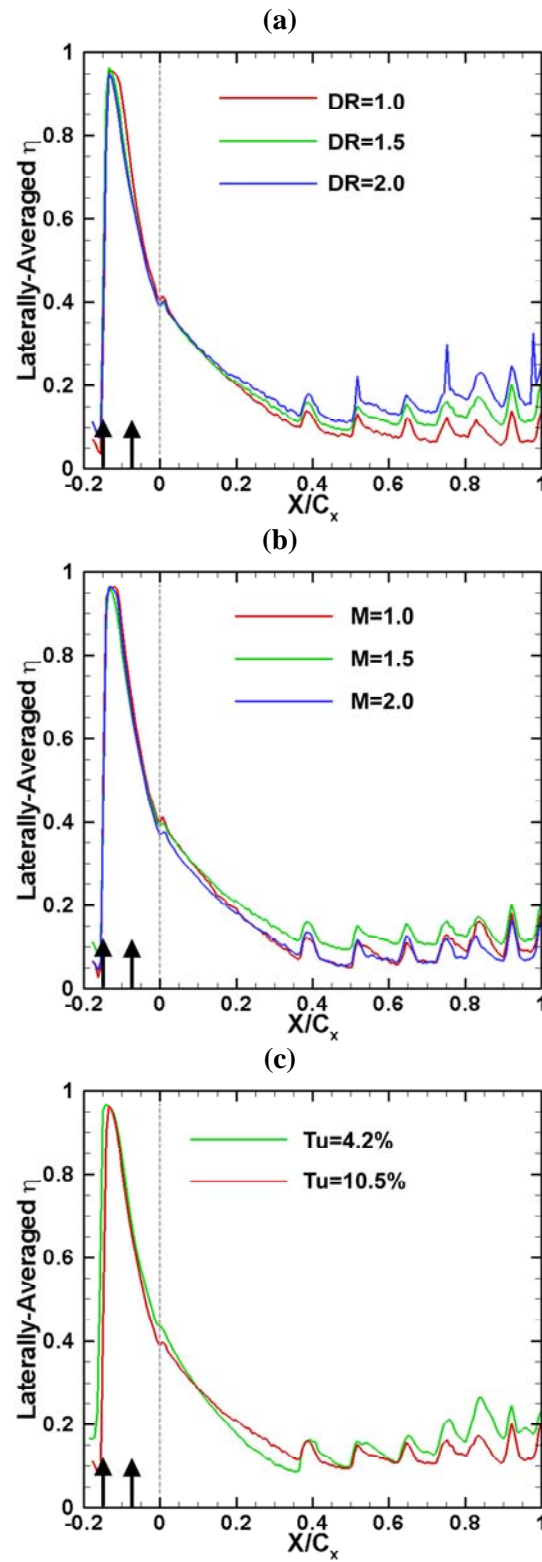


Figure 4.11 Laterally averaged effectiveness for Config. A (a) density ratio effect, (b) blowing ratio effect, (c) turbulence effect

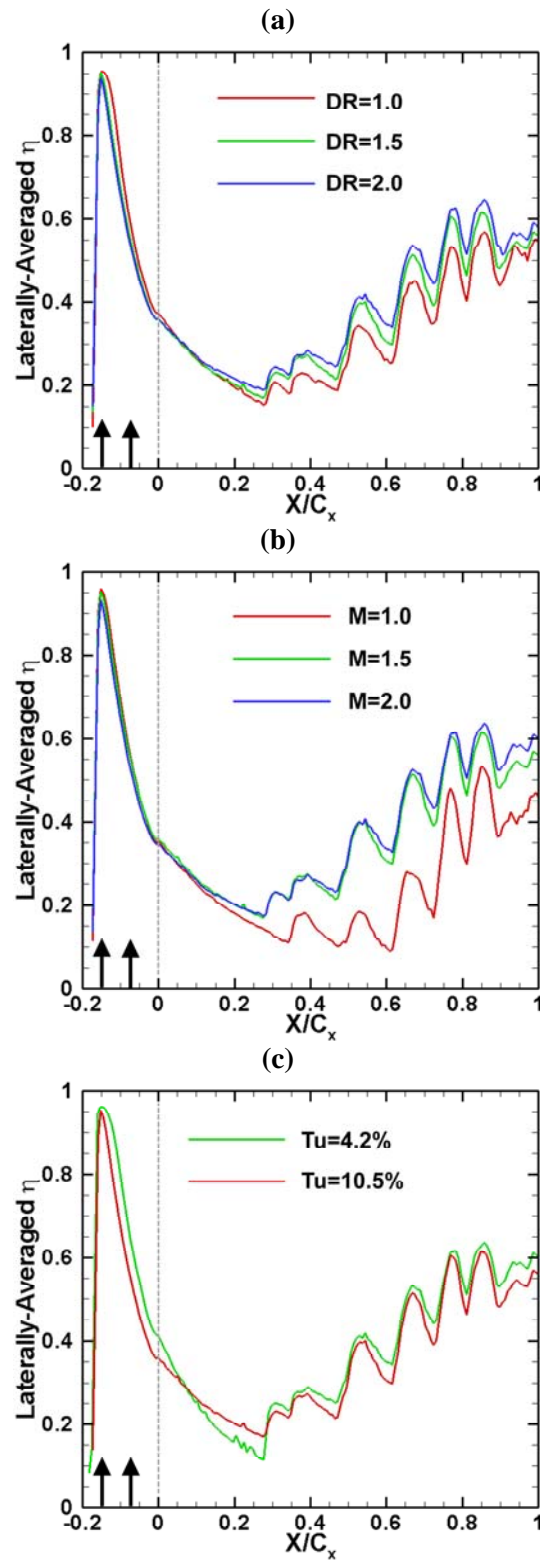


Figure 4.12 Laterally averaged effectiveness for Config. B (a) density ratio effect, (b) blowing ratio effect, (c) turbulence effect

4.4. Conclusions

An experimental study was undertaken to measure the film-cooling effectiveness on a turbine blade platform within a five-blade linear cascade. The platform is cooled by purge flow from a typical stator-rotor seal combined with discrete hole film-cooling. The key feature of this study is the use of high coolant density to simulate engine-like operating conditions. Some of the main highlights from the present study are presented below:

- 1) High coolant-to-mainstream density ratio results in higher effectiveness levels. However, the improvement of film-cooling is less significant for the shaped hole design.
- 2) The effectiveness for the shaped holes increases with increase of blowing ratio, whereas an optimal blowing ratio of 1.5 exists for the cylindrical holes.
- 3) Platform film-cooling effectiveness is a function of freestream turbulence level. Higher the freestream turbulence, lower the effectiveness.
- 4) Overall the shaped holes provide wider film coverage and higher effectiveness level than the cylindrical holes.
- 5) The pressure side corner of the platform remains a difficult region to cool. It requires a new design of film-cooling hole layout and a modification of platform, such as endwall contouring.

5. TURBINE BLADE TIP FILM-COOLING

5.1. Introduction

Large leakage flow occurs at the blade tip as a result of a high pressure differential from pressure to suction side. The hot leakage flow is the major cause of blade tip failures. To reduce the leakage flow and heat transfer on the tip, the blades of modern gas turbines typically have a recessed cavity at the tip and are called squealer tip blades. The groove acts as a labyrinth seal to increase flow resistance and thus reduces leakage flow.

Many recent studies conducted the studies in a cascade environment with squealer tip blade. Azad et al. [53] used transient liquid crystal technique to study the heat transfer on the first stage blade tip of an aircraft engine turbine (GE-E³). They compared squealer tip and plane tip geometry and concluded that the overall heat transfer coefficients were lower for squealer tip case. Azad et al. [54] also studied the effect of squealer geometry arrangement on gas turbine blade tip heat transfer and found that the location of the squealer rim could change the leakage flow and result in different heat loads to the blade tip. They also found that the suction side squealer provided best sealing to leakage flow among all the cases they studied. Kwak and Han [55, 56] examined heat transfer coefficient and film-cooling effectiveness on various film-cooling configurations and squealer tip geometries. Their results showed that the film-cooling effectiveness on the squealer tip was much higher than that on the plane tip. Chyu et al. [57] investigated heat transfer in a rectangular grooved tip model. They showed that the heat transfer in the

upstream end of the cavity was greatly reduced compared to the flat tip, however, at the downstream of the cavity, the heat transfer levels for the grooved tip were higher due to the reattachment inside the cavity.

5.2. Experimental Setup

The schematic view of the test section and the blow-down loop is shown in Figure 5.1. The test section consisted of a 5-blade linear cascade with blade tip profiles. A 3X scaled model of the GE-E³ blade is used with a blade span of 12.2cm and an axial chord length of 8.61cm. Figure 5.2 shows the blade profiles, the inlet and exit angles at design conditions. The blade tip and shroud definitions are also indicated in Figure 5.2. The test blade was made using stereo lithography (SLA). The four guide blades placed in the test section were made of aluminum.

Figure 5.3 shows the film-cooling measurement blade with the internal passage geometry. The passages are numbered from 1 to 6 with passage 1 closest to leading edge and passage 6 closest to trailing edge. Coolant is supplied to the test blade through two loops with three serpentine passages with a 3mm wall thickness in each loop. Figure 5.4 shows the geometry and orientation of the film-cooling holes on the pressure side and on the squealer blade tip. Ten cylindrical tip holes with a diameter of 1.27mm ($L/d=3.34$) are provided on the tip. Out of these ten holes, four are drilled such that they break out at 45° along the camber line of the blade on the cavity floor. The remaining six holes are drilled at 45° along a curve offset to the suction surface of the blade by 5.08 mm and are equally spaced by 18.3mm. The holes are inclined to the cavity floor in the direction of

the bulk fluid flow. The first five tip holes are connected to loop 1 (near LE) and the remaining five to loop 2 (near TE).

Nine film-cooling holes with a diameter of 1.27mm are located 9.5mm below the tip surface. The pressure side holes have a laidback and fan-shaped design expanding by 10° in the three directions (10° - 10° - 10°) with the expansion starting from the middle of the hole length, The hole-to-hole spacing is 8.9mm. The first three holes neat the leading edge are drilled at a radial angle of 45° to maximize the coolant spread whereas the remaining six holes are drilled at a compound angle of 45° to the blade span and 45° with respect to the airfoil pressure surface with $L/d=4$. The squealer tipped blade with recess of 2.1% of blade span is used in this study. The pressure side rim wall near the trailing edge is cutback by about 25% of the blade chord for the blade to allow accumulated coolant to escape.

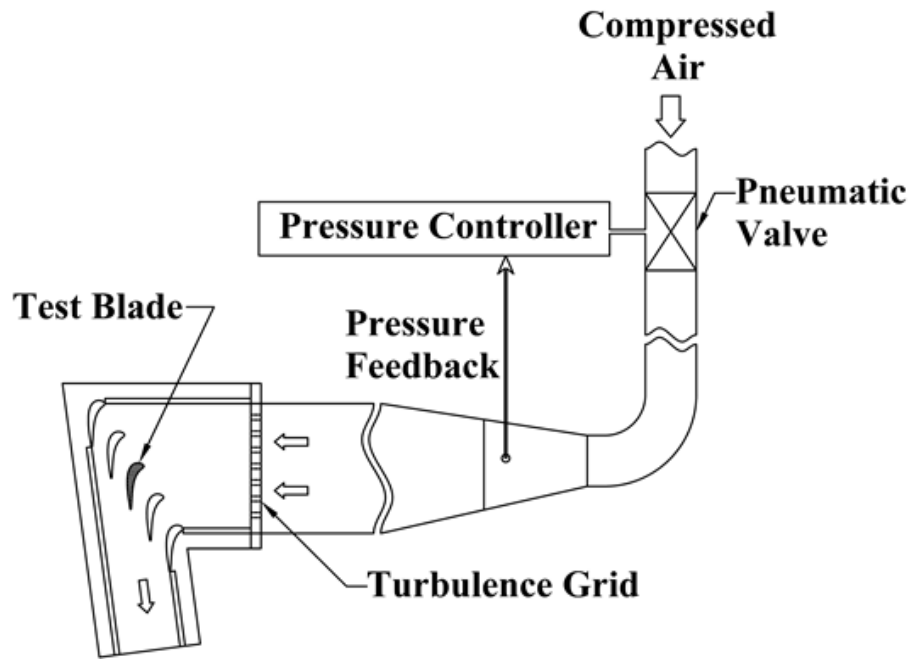


Figure 5.1 Schematic of test section and blow down facility

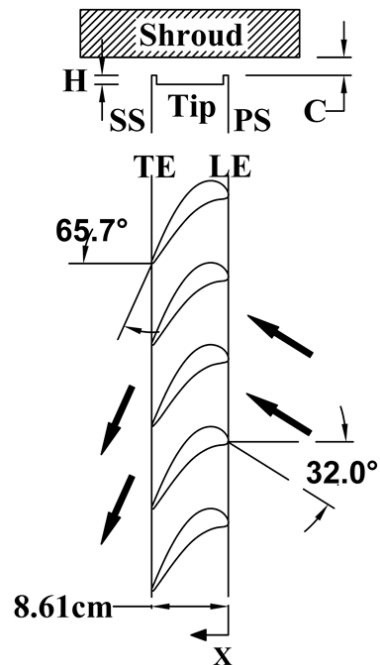
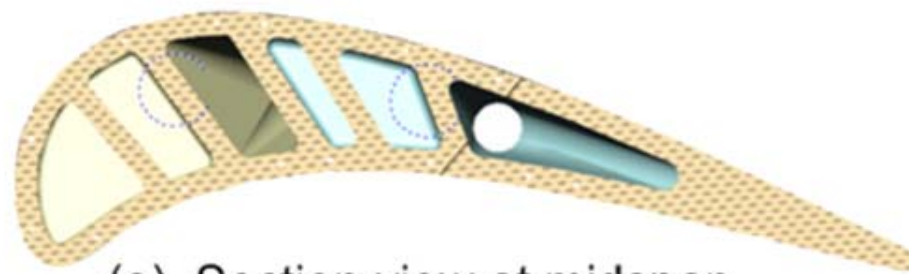
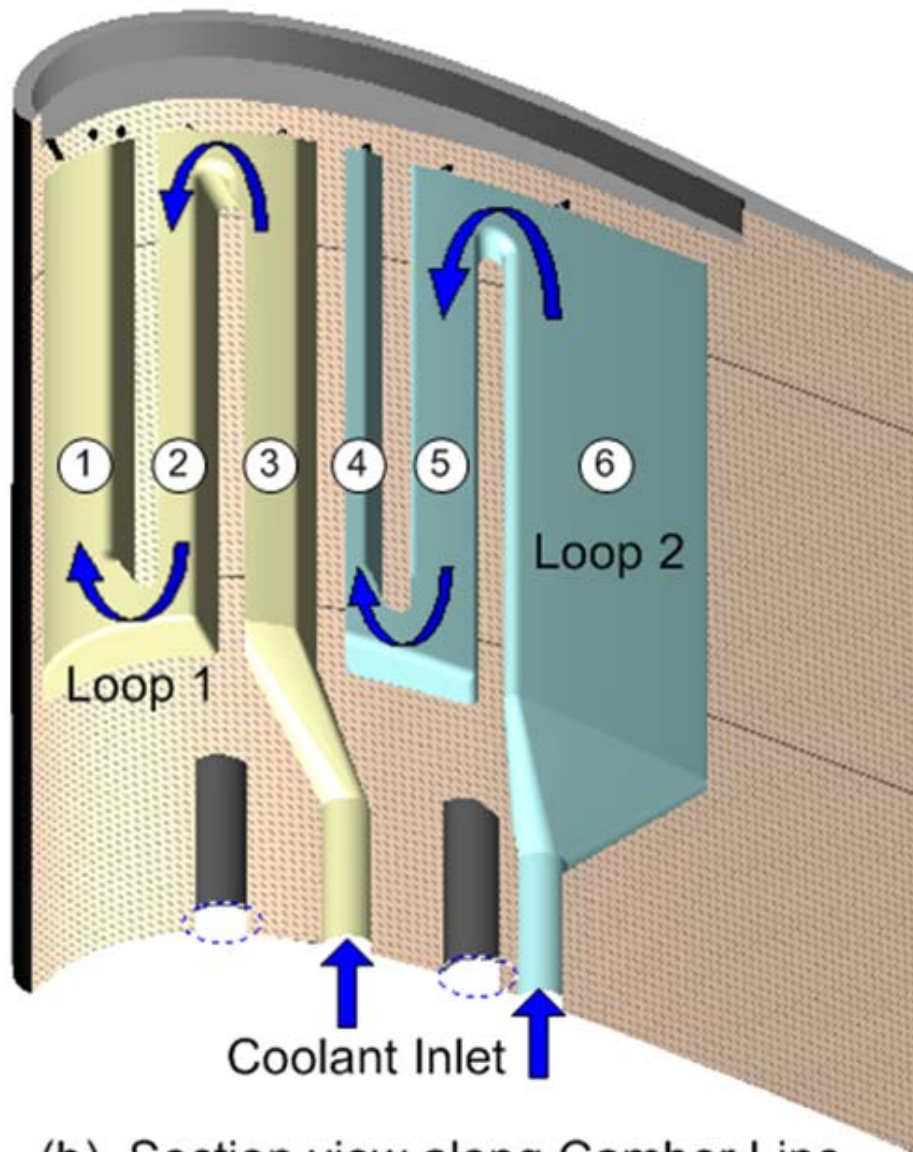


Figure 5.2 Definition of blade tip and shroud



(a) Section view at midspan



(b) Section view along Camber Line

Figure 5.3 Internal passage geometry of test blade

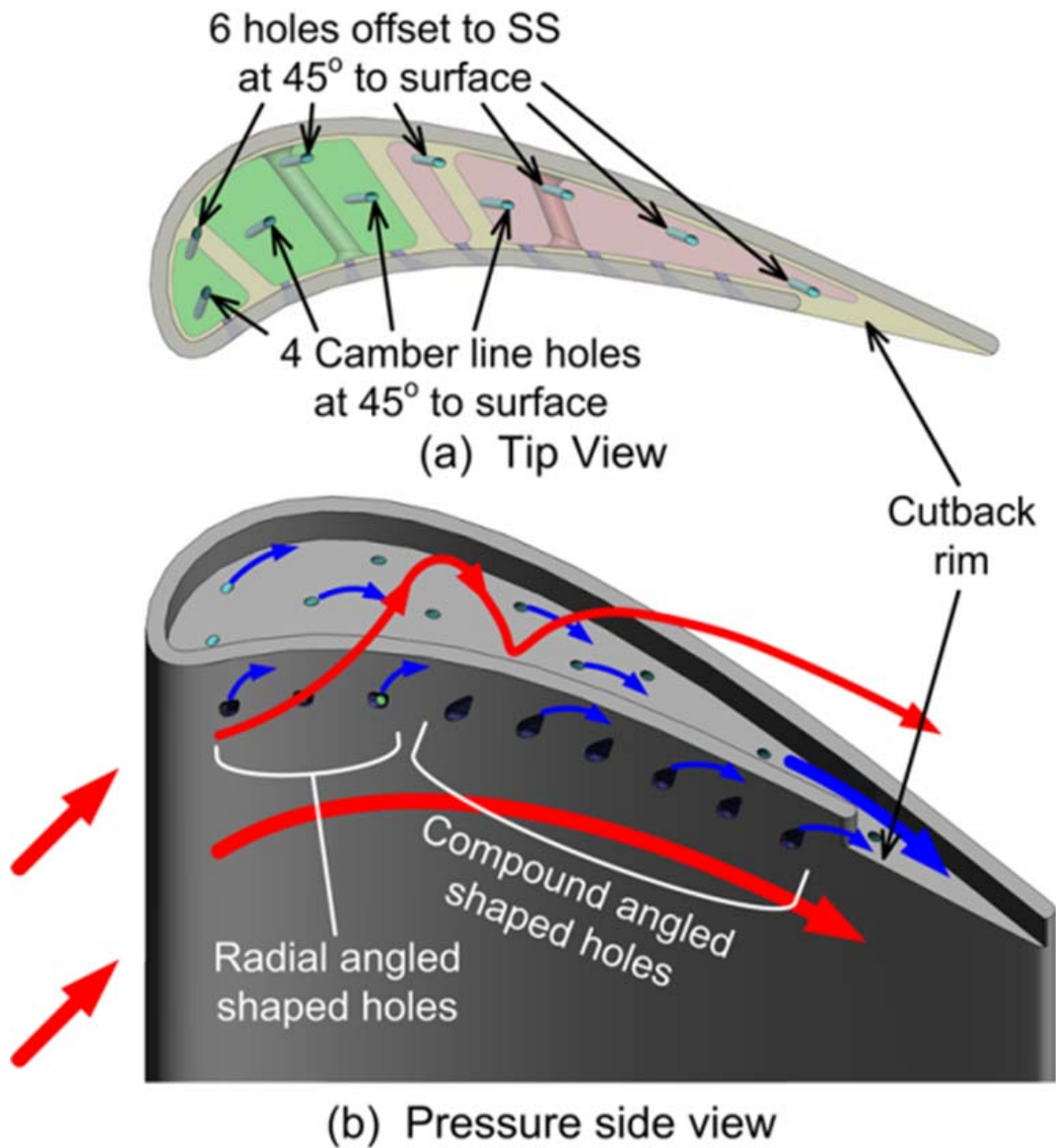


Figure 5.4 Orientation of tip and PS holes

5.3. Results and Discussion

5.3.1. Film-Cooling Effectiveness Results

Figure 5.5 shows the effectiveness results on squealer rims and cavity floor. On the cavity floor, the film coverage tends to be improving with the blowing ratio. Increase of blowing ratio from 1.0 to 1.5, the increase of effectiveness level is obvious; however, when the blowing ratio further increases to 2.0, the increase of effectiveness level is not significant. Jet lift-off can be observed around the holes near the leading edge at blowing ratio 2.0. Lift-off is indicated by a region of low effectiveness immediately downstream of the hole. Because the momentum of jet is too strong; it penetrates through the mainstream instead of forming a protection layer on the surface. As a result, effectiveness level decreases as blowing ratio elevates from 1.5 to 2.0 at the near leading edge portion.

5.3.2. Average Film-Cooling Effectiveness Results

Figure 5.6 shows the comparison of average film-cooling effectiveness obtained from the three blowing ratios along the axial chord. The average values are obtained by averaging the effectiveness magnitudes at a given x/C_x location. In general, the average effectiveness increases with increasing axial chord distance for all surfaces. The trend indicates that effectiveness increases with blowing ratio. Each spike represents the presence of a hole. Lift-off of the coolant jet can be observed for the holes closer to the leading edge as blowing ratio increases from 1.5 to 2.0 (up to $X/C_x=0.2$).

Figure 5.7 shows the area-averaged film-cooling effectiveness results. It can be noted that on the blade tip surface, effectiveness level increases with blowing ratio, $M = 2$ shows highest effectiveness.

5.4. Conclusions

A parametric study has been performed for measuring film-cooling effectiveness on a squealer blade tip with different blowing ratios. Effectiveness was measured on the cavity floor, rim, cavity rim walls and near tip pressure side. Effects of squealer cavity have been studied. Major findings from the experimental results are listed below:

- 1) In general, higher blowing ratios give higher effectiveness on the blade tip, $M = 2.0$ shows best results.
- 2) The cutback squealer rim results in high effectiveness in the trailing edge region of the blade tip as compared to a full squealer.
- 3) Coolant accumulation results in increasing effectiveness from blade leading edge to trailing edge.

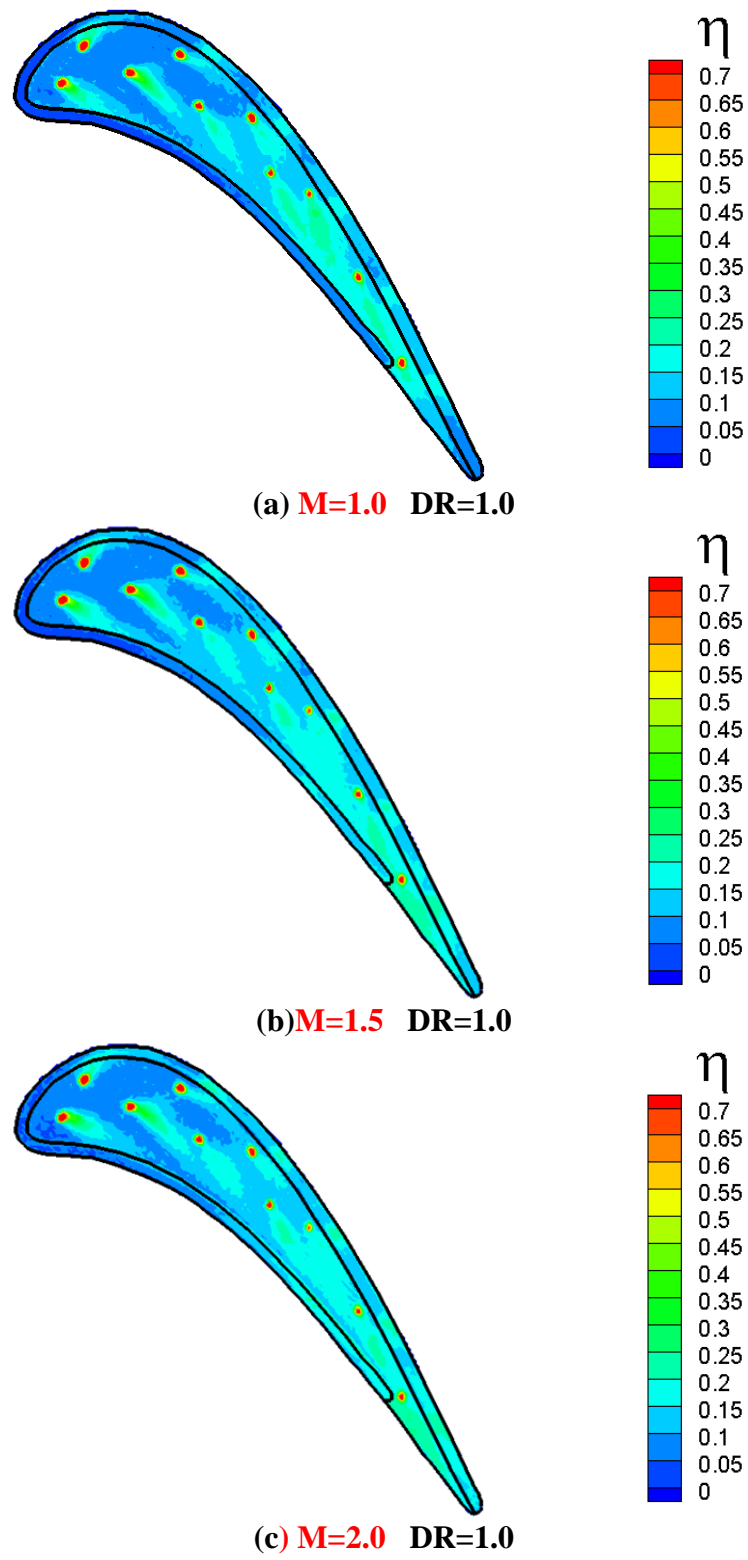


Figure 5.5 Film-Cooling effectiveness distribution on blade tip

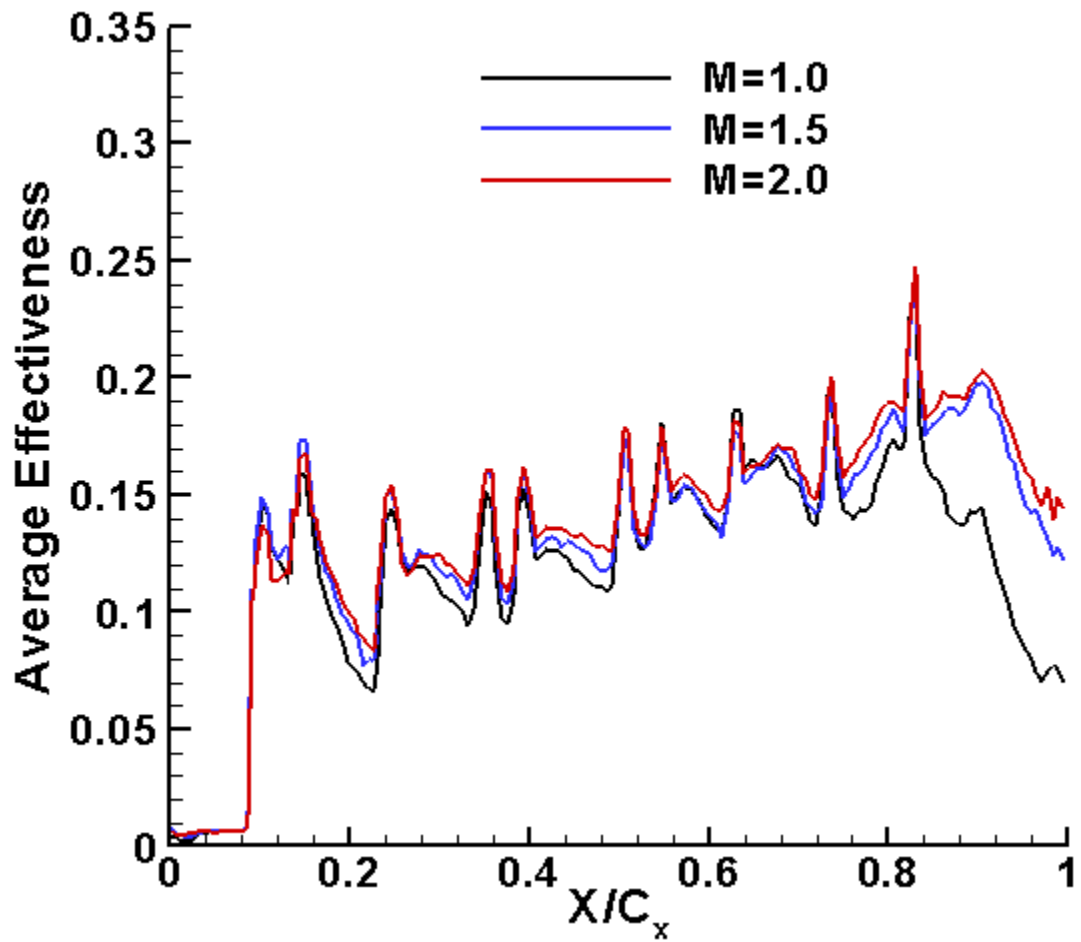


Figure 5.6 Averaged film-cooling effectiveness from experimental results

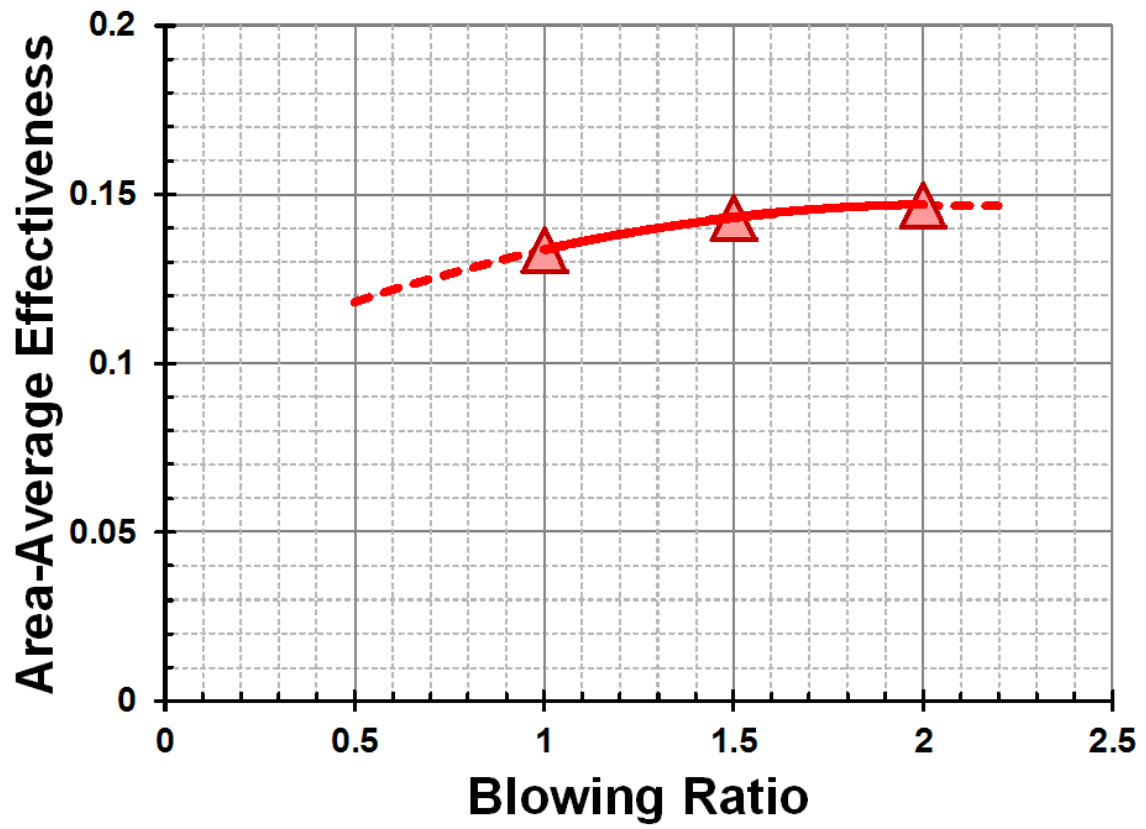


Figure 5.7 Area-averaged film-cooling effectiveness from experimental results

6. VANE SUCTION SIDE HEAT TRANSFER STUDY

6.1. Objectives of Vane Suction Side Heat Transfer

This research is to study the effect of transonic flow on turbine vane suction side heat transfer without film-cooling using a Transient Liquid Crystal (TLC) method. Tests were performed in a five-vane annular cascade with a blow-down flow loop facility. The exit Mach numbers are controlled to be about 1.1, the test vane features 3 rows of radial-angle cylindrical holes around the leading edge, and 2 rows of compound-angle shaped holes on the suction side.

6.2. Test Facilities for Heat Transfer Study

A scaled model of the Honeywell vane was placed in the center of annular cascade. Test vane was manufactured by Stereolithography (SLA) process. Figure 6.1(a) shows the unique shape and cooling hole locations of the vane. It has a various height converges from leading to trailing edge. The leading edge of the test vane is equipped with three rows of showerhead film cooling holes; the middle row is aligned with the stagnation line. Three leading edge rows are staggered with respect to one another. Each showerhead row has 7 radial-angle cylindrical holes with a hole-to-hole spacing of $s/d = 6.9$. Two row of compound-angle shaped holes (SS1, SS2) on the suction side with a hole-to-hole spacing of $s/d = 7.3$. The shaped holes have a typical design of metering length and expansion angle in three directions. Coolant is delivered from three straight passages as shown in Figure 6.1(b). Flow in each passage is individually controlled by a rotameter, the schematic setup is shown in Figure 6.2.

During the blow-down test, the cascade exit air velocities were set at exit Mach number ($Ma_{\text{exit}} = 1.1$). The exit velocity was continuously monitored using a Pitot-static pressure probe placed downstream of the cascade. The blowdown facility could maintain steady flow in the cascade for about 30 seconds. Compressed air stored in tanks entered a high flow digital control valve, which could maintain steady flow receiving downstream pressure feedback. The control valve could maintain a velocity within 2% of desired value. A grid was placed upstream of the cascade and generated turbulence level of 10% at test section inlet. The average length scale was approximately 1.5cm.

To monitor the exit velocity, a Pitot-static probe is stationed 75% C_x distance downstream of the test vane. Before applying liquid crystal to the test surface, it is coated with black paint. The black paint acts as a binder; neighboring vanes and the passages are also sprayed black to eliminate any stray reflection.

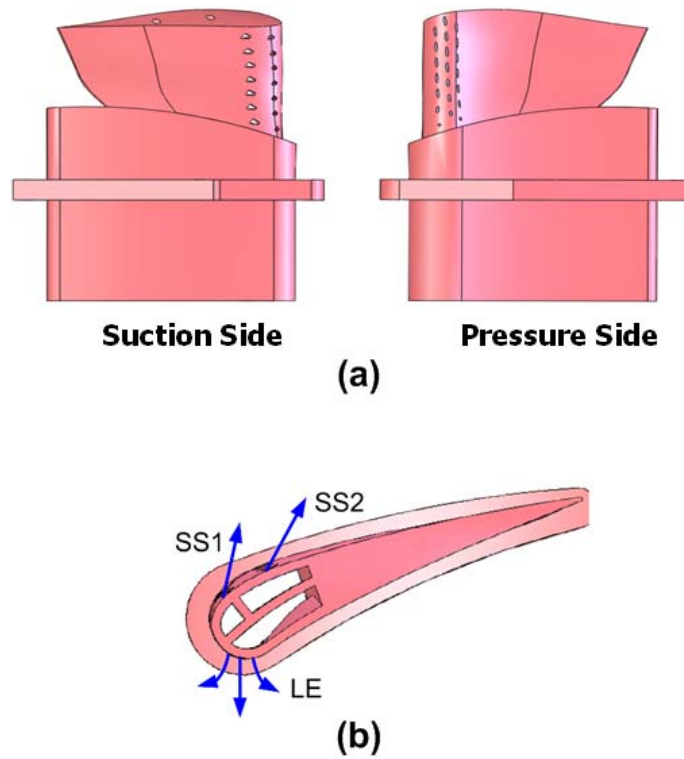


Figure 6.1 Test Vane (a) hole locations (b) coolant passage

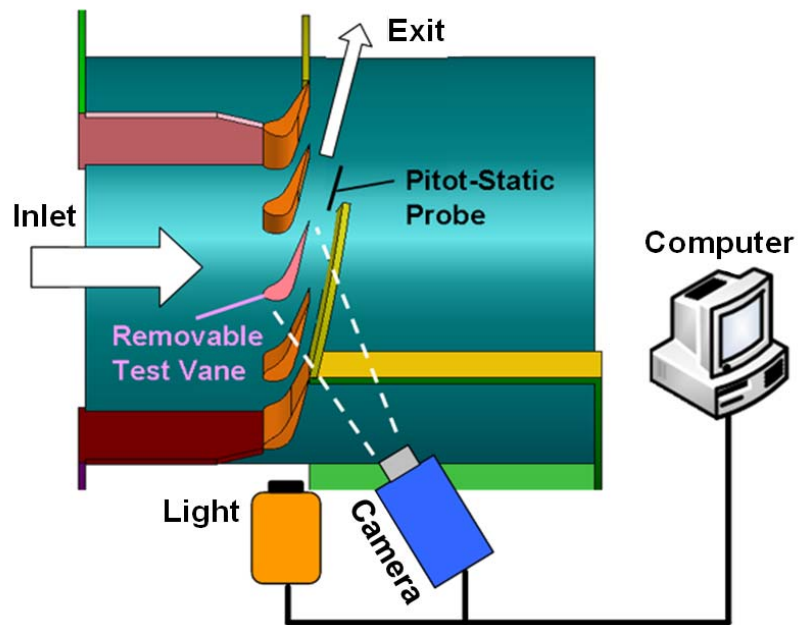


Figure 6.2. Schematic of setup for vane suction side film-cooling and heat transfer study

6.3. Results and Discussion

6.3.1. Surface Initial Temperature

The heat transfer coefficients are measured by recording the changing vane temperature and time using the transient liquid crystal technique. To perform the transient heat transfer test, the stator vane is preheated before the run. The vane was heated slowly until the surface temperature was in the range of 50°C-60°C. Three thermocouples mounted inside the vane internal coolant passages served as guide during the heating process. The initial suction surface temperature (T_i) is shown in Figure 6.3. As soon as the vane reaches the pre-set thermocouple temperatures, the heating procedure stops and the mainstream air is let in.

6.3.2. Heat Transfer Coefficient Results

The mainstream temperature is kept at a constant value of 20°C although the true representative of mainstream flow temperature is the adiabatic surface temperature. Also in the present calculations, a constant thermal conductivity of 0.47 W/m-K (20°C) was used. Figure 6.4 shows the heat transfer coefficient contour plot on the vane suction surface obtained from experiment. Due to the limitation of viewing window, region before $X/L=0.1$ and region after $X/L=0.7$ are excluded. Results show that the heat transfer coefficients increase toward the trailing edge (or throat) as flow accelerates. A spanwise variation can be found due to passage and horseshoe vortices (i.e., endwall effect). There are high heat transfer region before $X/L=0.1$ at the leading edge, followed by a low heat transfer region where flow is developing and becoming transition.

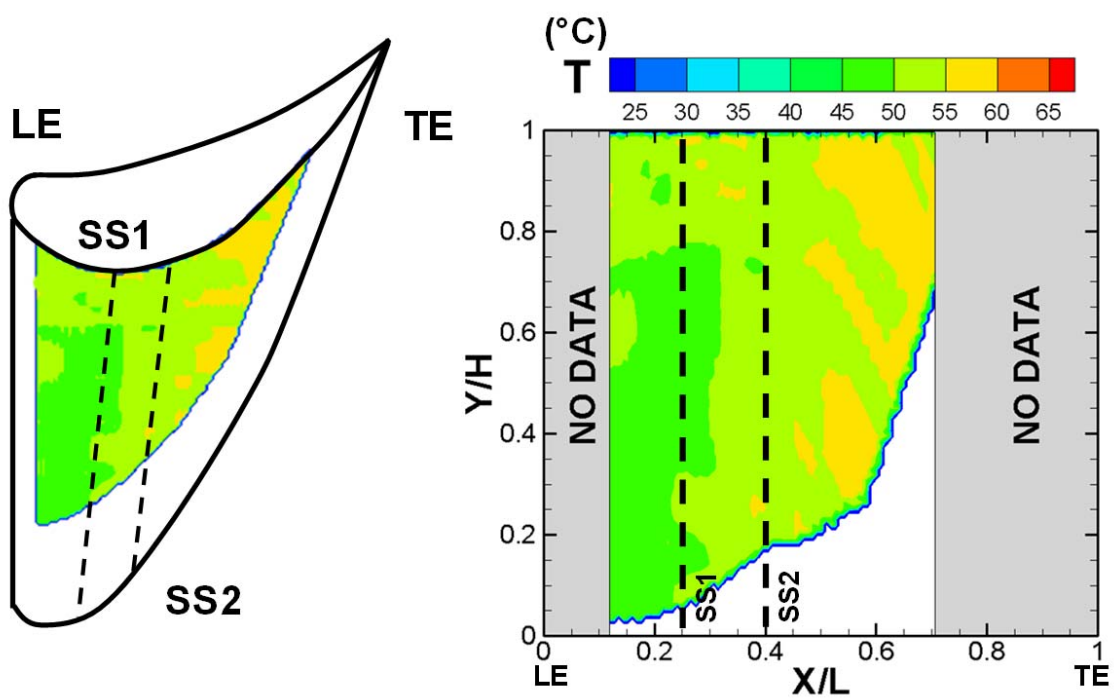


Figure 6.3. Initial temperature on stator vane suction side

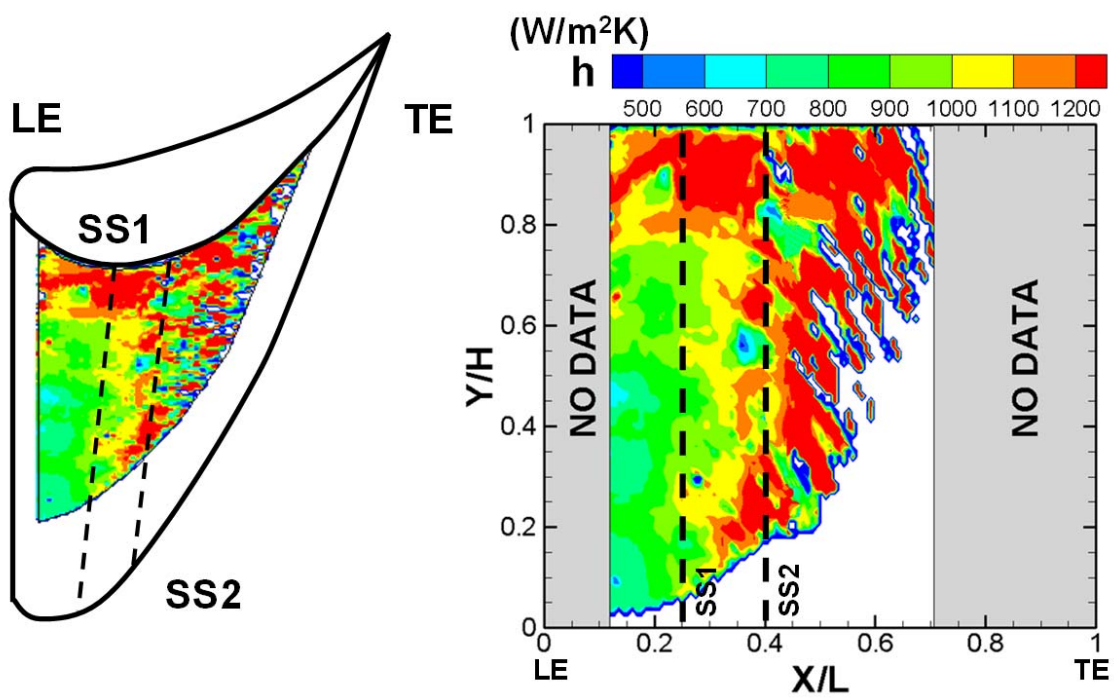


Figure 6.4. Heat transfer coefficient on the vane suction side

6.4. Conclusions

A heat transfer study on the stator vane suction surface was performed using transient heat transfer method. Major findings from the experimental results are listed below:

- 1) Heat transfer coefficients increase toward the trailing edge (or throat).
- 2) A low heat transfer region was discovered at $X/L=0.15$ where separation occurs.
- 3) Spanwise heat transfer variation may be due to passage and horseshoe vortices.

7. SUMMARY

Gas turbines are widely used in aircraft propulsion and land-based power generation or industrial applications, so it is vital these engines operate as efficiently as possible. Thermal efficiency and power output of gas turbine increase with increasing turbine rotor inlet temperatures; the operating temperatures are far above the permissible metal temperatures. Advanced cooling technologies must be applied to the airfoils so they can withstand these extreme conditions. To increase the life of the turbine blades and vanes, they must be cooled. These components are cooled by extracting gas from the engine's compressor, and circulating this "coolant" gas through the hollow airfoils. The coolant gas removes heat from the walls of the blades and vanes, so they can survive in the engine. However, excessive use of coolant discharged from the compressor reduces engine performance. Thus much research has been conducted to understand the physical phenomena regarding the film-cooling process and to find better configurations that can provide more protection with less coolant. The present study contains both film-cooling effectiveness and heat transfer on gas turbine blade. Experimental investigations were performed for four different test sections involving the study of film-cooling and heat transfer.

For the film-cooling study, film-cooling effectiveness results were obtained for a gas turbine blade span, platform, and tip. The Pressure Sensitive Paint (PSP) technique was employed to study this phenomenon. The PSP technique is free from errors related to heat conduction frequently encountered in other heat transfer measurement techniques. As a result, clear coolant traces were observed with accurate data near the

ejection holes. Parametric investigations were performed to optimize the blade film coverage and innovative ideas were tested. The effect of blowing ratio, density ratio, freestream turbulence intensity, and film-cooling hole geometries were investigated.

For the heat transfer study, experiments were performed in a partial annular cascade with transonic exit flow condition. Heat transfer coefficient on the stator vane suction side surface was examined by using transient liquid crystal method. This test investigates the effect of transonic flow on turbine vane suction side heat transfer as very limited data exists in open literature in this area.

REFERENCES

- [1] Han, J. C., Dutta, S., and Ekkad, S., 2000, *Gas Turbine Heat Transfer and Cooling Technology*, Taylor & Francis, New York.
- [2] McLachlan, B., and Bell, J., 1995, "Pressure-Sensitive Paint in Aerodynamic Testing," *Experimental Thermal and Fluid Science*, **10**(4), pp. 470-485.
- [3] Wright, L., Gao, Z., Varvel, T., and Han, J., 2005, "Assessment of Steady State PSP, TSP, and IR Measurement Techniques for Flat Plate Film Cooling," ASME Paper HT-2005-72363, pp. 37-46.
- [4] Kline, S. J., and McClintock, F., 1953, "Describing Uncertainties in Single-Sample Experiments," *Journal of Mechanical Engineering*, **75**(1), pp. 3-8.
- [5] Coleman, H. W., and Steele, W. G., 1999, *Experimentation and Uncertainty Analysis for Engineers*, John Wiley & Sons, New York.
- [6] Goldstein, R., Eckert, E., and Burggraf, F., 1974, "Effects of Hole Geometry and Density on Three-Dimensional Film Cooling," *International Journal of Heat and Mass Transfer*, **17**(5), pp. 595-607.
- [7] Thole, K., Gritsch, M., Schulz, A., and Wittig, S., 1998, "Flowfield Measurements for Film-Cooling Holes with Expanded Exits," *Journal of Turbomachinery*, **120**, pp. 327-335.
- [8] Yu, Y., Yen, C. H., Shih, T. I. P., Chyu, M., and Gogineni, S., 2002, "Film Cooling Effectiveness and Heat Transfer Coefficient Distributions around Diffusion Shaped Holes," *Journal of Heat Transfer*, **124**, pp. 820-827.

- [9] Dittmar, J., Schulz, A., and Wittig, S., 2003, "Assessment of Various Film-Cooling Configurations Including Shaped and Compound Angle Holes Based on Large-Scale Experiments," *Journal of Turbomachinery*, **125**, pp. 57-64.
- [10] Ito, S., Goldstein, R., and Eckert, E., 1977, "Film Cooling of a Gas Turbine Blade," *Journal of Engineering for Gas Turbines and Power*, **113**, pp. 476-481.
- [11] Chen, P. H., Hung, M. S., and Ding, P. P., 2001, "Film Cooling Performance on Curved Walls with Compound Angle Hole Configuration," *Annals of the New York Academy of Sciences*, **934**(1), pp. 353-360.
- [12] Bunker, R. S., 2005, "A Review of Shaped Hole Turbine Film-Cooling Technology," *Journal of Heat Transfer*, **127**, pp. 441-453.
- [13] Ekkad, S., Mehendale, A., Han, J., and Lee, C., 1997, "Combined Effect of Grid Turbulence and Unsteady Wake on Film Effectiveness and Heat Transfer Coefficient of a Gas Turbine Blade With Air and CO₂ Film Injection," *Journal of Turbomachinery*, **119**, pp. 594-600.
- [14] Wayne, S. K., and Bogard, D. G., 2007, "High-Resolution Film Cooling Effectiveness Comparison of Axial and Compound Angle Holes on the Suction Side of a Turbine Vane," *Journal of Turbomachinery*, **129**, pp. 202-211.
- [15] Dorrington, J. R., Bogard, D. G., and Bunker, R. S., 2007, "Film Effectiveness Performance for Coolant Holes Imbedded in Various Shallow Trench and Crater Depressions," ASME Paper GT2007-27992, pp. 749-758.

- [16] Wayne, S. K., and Bogard, D. G., 2007, "High-Resolution Film Cooling Effectiveness Measurements of Axial Holes Embedded in a Transverse Trench with Various Trench Configurations," *Journal of Turbomachinery*, **129**, pp. 294-302.
- [17] Colban, W. F., Thole, K. A., and Bogard, D., 2011, "A Film-Cooling Correlation for Shaped Holes on a Flat-Plate Surface," *Journal of Turbomachinery*, **133**, pp. 011002-011012.
- [18] Mhetras, S., Narzary, D., Gao, Z., and Han, J. C., 2008, "Effect of a Cutback Squealer and Cavity Depth on Film-Cooling Effectiveness on a Gas Turbine Blade Tip," *Journal of Turbomachinery*, **130**, pp. 021002-021014.
- [19] Ou, S., Han, J. C., Mehendale, A. B., and Lee, C., 1994, "Unsteady Wake Over a Linear Turbine Blade Cascade With Air and CO₂ Film Injection: Part I - Effect on Heat Transfer Coefficients," *Journal of Turbomachinery*, **116**, pp. 721-729.
- [20] Rigby, M., Johnson, A., and Oldfield, M., 1990, "Gas Turbine Rotor Blade Film Cooling with and without Simulated NGV Shock Waves and Wakes," ASME Paper 90-GT-78, pp. 190-197.
- [21] Langston, L., 1980, "Crossflows in a Turbine Cascade Passage," *Journal of Engineering for Power*, **120**, pp. 866-874.
- [22] Wang, H., Olson, S., Goldstein, R., and Eckert, E., 1997, "Flow Visualization in a Linear Turbine Cascade of High Performance Turbine Blades," *Journal of Turbomachinery*, **119**, pp. 1-9.

- [23] Gao, Z., Narzary, D. P., and Han, J. C., 2009, "Film-Cooling on a Gas Turbine Blade Pressure Side or Suction Side With Compound Angle Shaped Holes," *Journal of Turbomachinery*, **131**, pp. 011019-011029.
- [24] Narzary, D. P., Liu, K. C., Rallabandi, A. P., and Han, J. C., 2012, "Influence of Coolant Density on Turbine Blade Film-Cooling Using Pressure Sensitive Paint Technique," *Journal of Turbomachinery*, **134**, pp. 031006-031015.
- [25] Schmidt, D., and Bogard, D., 1996, "Effects of Free-Stream Turbulence and Surface Roughness on Film Cooling," *ASME Paper 96-GT-462*, pp. 814-825.
- [26] Drost, U., Bölcs, A., and Hoffs, A., 1997, "Utilization of the Transient Liquid Crystal Technique for Film Cooling Effectiveness and Heat Transfer Investigations on a Flat Plate and a Turbine Airfoil," *ASME Paper 98-GT-483*, pp. 9-17.
- [27] Ethridge, M. I., Cutbirth, J. M., and Bogard, D. G., 2001, "Scaling of Performance for Varying Density Ratio Coolants on an Airfoil with Strong Curvature and Pressure Gradient Effects," *Journal of Turbomachinery*, **123**, pp. 231-237.
- [28] Takeishi, K., Matsuura, M., Aoki, S., and Sato, T., 1990, "An Experimental Study of Heat Transfer and Film Cooling on Low Aspect Ratio Turbine Nozzles," *Journal of Turbomachinery*, **112**, pp. 488-496.
- [29] Jabbari, M., Marston, K., Eckert, E., and Goldstein, R., 1996, "Film Cooling of the Gas Turbine Endwall by Discrete-Hole Injection," *Journal of Turbomachinery*, **118**, pp. 278-284.

- [30] Friedrichs, S., Hodson, H., and Dawes, W., 1996, "Distribution of Film-Cooling Effectiveness on a Turbine Endwall Measured Using the Ammonia and Diazo Technique," *Journal of Turbomachinery*, **118**(4), pp. 613-621.
- [31] Friedrichs, S., Hodson, H., and Dawes, W., 1999, "The Design of an Improved Endwall Film-Cooling Configuration," *Journal of Turbomachinery*, **121**, pp. 772-780.
- [32] Vogel, G., Wagner, G., and Böles, A., 2002, "Transient Liquid Crystal Technique Combined with PSP for Improved Film Cooling Measurements," 10th International Symposium on Flow Performance, pp. 630-639.
- [33] Barigozzi, G., Benzoni, G., Franchini, G., and Perdichizzi, A., 2006, "Fan-Shaped Hole Effects on the Aero-Thermal Performance of a Film-Cooled Endwall," *Journal of Turbomachinery*, **128**, pp. 43-52.
- [34] Granser, D., and Schulenberg, T., 1990, "Prediction and Measurement of Film Cooling Effectiveness for a First-Stage Turbine Vane Shroud," ASME Paper 90-GT-95, pp. 1990-1998.
- [35] Roy, R., Squires, K., Gerendas, M., Song, S., Howe, W., and Ansari, A., 2000, "Flow and Heat Transfer at the Hub Endwall of Inlet Vane Passages - Experiments and Simulations," ASME Paper 2000-GT-198, pp. 8-17.
- [36] Burd, S. W., Satterness, C., and Simon, T., 2000, "Effects of Slot Bleed Injection Over a Contoured Endwall On Nozzle Guide Vane Cooling Performance: Part II- Thermal Measurements," ASME Paper 2000-GT-200, pp. 200-211.

- [37] Oke, R., Simon, T., Shih, T., Zhu, B., Lin, Y. L., and Chyu, M., 2001, "Measurements Over a Film-Cooled, Contoured Endwall with Various Coolant Injection Rates," ASME Paper 2001-GT-0140, pp. 140-149.
- [38] Oke, R. A., and Simon, T. W., 2002, "Film Cooling Experiments with Flow Introduced Upstream of a First Stage Nozzle Guide Vane Through Slots of Various Geometries," ASME Paper GT2002-30169, pp. 33-40.
- [39] Zhang, L. J., and Jaiswal, R. S., 2001, "Turbine Nozzle Endwall Film Cooling Study Using Pressure-Sensitive Paint," *Journal of Turbomachinery*, **123**, pp. 730-738.
- [40] Zhang, L., and Moon, H. K., 2003, "Turbine Nozzle Endwall Inlet Film Cooling: The Effect of a Back-Facing Step," ASME Paper GT2003-38319, pp. 203-211.
- [41] Wright, L. M., Blake, S. A., Rhee, D. H., and Han, J. C., 2009, "Effect of Upstream Wake With Vortex on Turbine Blade Platform Film Cooling With Simulated Stator-Rotor Purge Flow," *Journal of Turbomachinery*, **131**, pp. 021017-021026.
- [42] Suryanarayanan, A., Ozturk, B., Schobeiri, M., and Han, J., 2010, "Film Cooling Effectiveness on a Rotating Turbine Platform Using Pressure Sensitive Paint Technique," *Journal of Turbomachinery*, **132**(4), pp. 041001-041013.
- [43] Nicklas, M., 2001, "Film-Cooled Turbine Endwall in a Transonic Flow Field: Part II - Heat Transfer and Film-Cooling Effectiveness," *Journal of Turbomachinery*, **123**, pp. 720-729.
- [44] Wright, L. M., Blake, S. A., and Han, J. C., 2008, "Film Cooling Effectiveness Distributions on a Turbine Blade Cascade Platform With Stator-Rotor Purge and Discrete Film Hole Flows," *Journal of Turbomachinery*, **130**, pp. 031015-031014.

- [45] Suryanarayanan, A., Mhetras, S., Schobeiri, M., and Han, J., 2009, "Film-Cooling Effectiveness on a Rotating Blade Platform," *Journal of Turbomachinery*, **131**, pp. 011014-011025.
- [46] Kadotani, K., and Goldstein, R., 1979, "On the Nature of Jets Entering a Turbulent Flow Part A : Jet-Mainstream Interaction," *Journal of Engineering for Power*, **101**, pp. 459-465.
- [47] Jumper, G., Elrod, W., and Rivir, R., 1991, "Film Cooling Effectiveness in High-Turbulence Flow," *Journal of Turbomachinery*, **113**, pp. 479-483.
- [48] Bons, J. P., MacArthur, C. D., and River, R. B., 1996, "The Effect of High Free-Stream Turbulence on Film Cooling Effectiveness," *Journal of Turbomachinery*, **118**(4), pp. 814-825.
- [49] Colban, W., Thole, K., and Haendler, M., 2008, "A Comparison of Cylindrical and Fan-Shaped Film-Cooling Holes on a Vane Endwall at Low and High Freestream Turbulence Levels," *Journal of Turbomachinery*, **130**, pp. 031007-031016.
- [50] Gao, Z., Narzary, D., and Han, J. C., 2009, "Turbine Blade Platform Film Cooling With Typical Stator-Rotor Purge Flow and Discrete-Hole Film Cooling," *Journal of Turbomachinery*, **131**, pp. 041004-041014.
- [51] Gao, Z., Narzary, D., Mhetras, S., and Han, J. C., 2007, "Upstream Vortex Effects on Turbine Blade Platform Film Cooling With Typical Stator-Rotor Purge Flow," *ASME Paper IMECE-2007-41717*, pp. 707-718.
- [52] Narzary, D. P., Liu, K. C., and Han, J. C., 2009, "Influence of Coolant Density on Turbine Blade Platform Film-Cooling," *ASME Paper GT2009-59342*, pp. 287-299

- [53] Azad, G. S., Han, J. C., Teng, S., and Boyle, R. J., 2000, "Heat Transfer and Pressure Distributions on a Gas Turbine Blade Tip," *Journal of Turbomachinery*, **122**, pp. 717-724.
- [54] Azad, G. S., Han, J. C., and Boyle, R. J., 2000, "Heat Transfer and Flow on the Squealer Tip of a Gas Turbine Blade," *Journal of Turbomachinery*, **122**, pp. 725-732.
- [55] Kwak, J. S., and Han, J. C., 2002, "Heat Transfer Coefficient and Film-Cooling Effectiveness on a Gas Turbine Blade Tip," ASME Paper GT2002-30194, pp. 309-318.
- [56] Kwak, J. S., and Han, J. C., 2002, "Heat Transfer Coefficient and Film-Cooling Effectiveness on the Squealer Tip of a Gas Turbine Blade," ASME Paper GT2002-30555 pp. 1073-1082.
- [57] Chyu, M., Moon, H., and Metzger, D., 1989, "Heat Transfer in the Tip Region of Grooved Turbine Blades," *Journal of Turbomachinery*, **111**, pp. 131-138.

VITA

Name: Kevin Liu

Address: c/o Dr. Je-Chin Han,

Department of Mechanical Engineering,

TAMU 3123, College Station, TX, 77843-3123

Email: qmore@tamu.edu

Education: B.S., Mechanical and Nuclear Engineering, Kansas State University, 2007

M.S., Mechanical Engineering, Texas A&M University, 2009

Ph.D., Mechanical Engineering, Texas A&M University, 2012